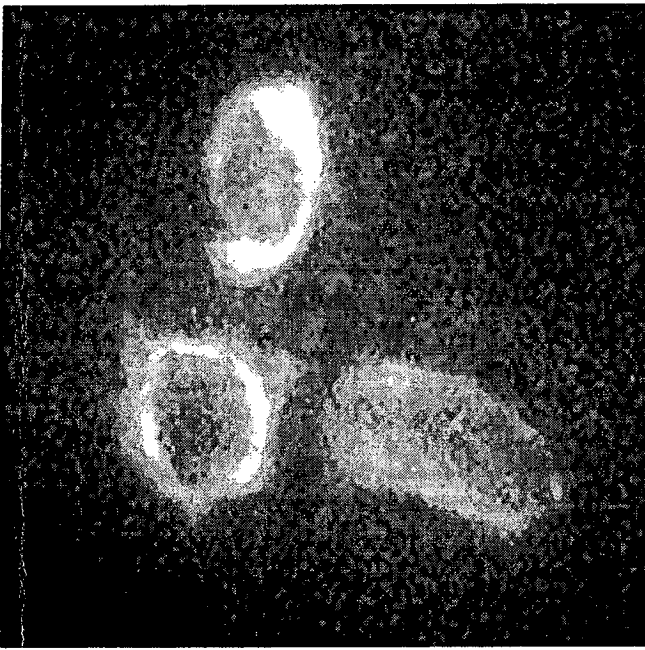


Rhodes College Digital Archives - DLynx

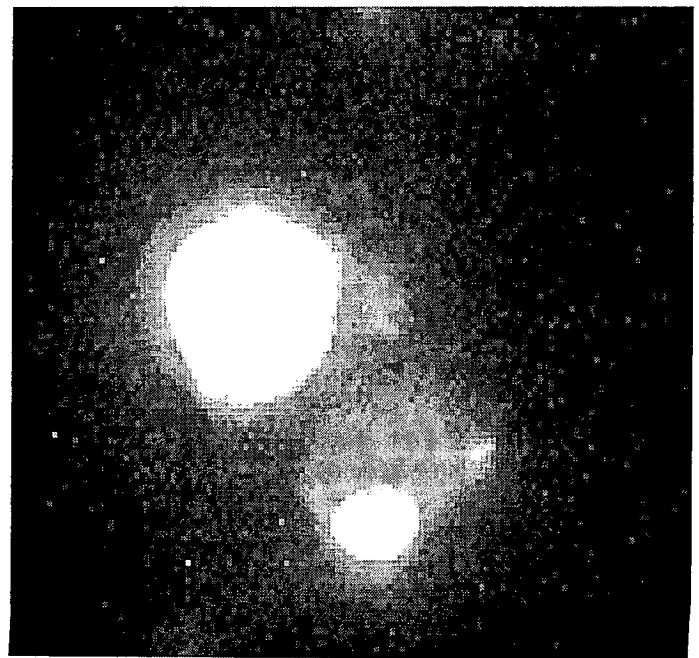
Rhodes Journal of Biological Science Volume 20, Spring 2003

Item Type	Other
Publisher	Memphis, Tenn. : Students of the Department of Biology, Rhodes College
Rights	Rhodes College owns the rights to the archival digital objects in this collection. Objects are made available for educational use only and may not be used for any non-educational or commercial purpose. Approved educational uses include private research and scholarship, teaching, and student projects. For additional information please contact archives@rhodes.edu . Fees may apply.
Download date	2026-04-11 23:03:54
Link to Item	http://hdl.handle.net/10267/13653



The Rhodes Journal of Biological Sciences

Volume XX
Spring 2003



The Rhodes Journal of Biological Science

VOLUME XX Spring 2003

Statement of Purpose:

The Rhodes Journal of Biological Sciences is a student-edited, annual publication which recognizes the scientific achievements of Rhodes students. Founded seventeen years ago as a scholarly forum for student research and scientific ideas, the journal aims to maintain and stimulate the tradition of independent study. We hope that in reading the journal, other students will be encouraged to pursue scientific investigations and research.

Editors

Katie Jameson
Ann Young

Acknowledgements: The editors would like to thank Dr. Jay Blundon for his invaluable support and assistance.

**RHODES COLLEGE
DEPARTMENT OF BIOLOGY
2000 NORTH PARKWAY
MEMPHIS, TN 38112-1699
(901) 843-3555
www.rhodes.edu/biology**

The Rhodes Journal of Biological Sciences
VOL. XX

Table of Contents

Original Studies

An Analysis of the Fibrilization of p53tet-R337H and p53tet-WT Prentice L. Bowman '04	1-7
Functional analysis of EBNA-3C required for regulation of the EBV oncoprotein LMP-1 Courtney Frye '05	8-23
Investigation into the Herpes Simplex Virus Type 1 Alison Groeger '04	24-35
Impact of Water Lilies (<i>Nymphaea tuberosa</i>) on Predator-Avoidance Behavior of <i>Daphnia magna</i> Lisa M. Harsch '05	36-60
Activation of GABA-B Receptors Attenuates N-type and Facilitates L-type Calcium Currents in Isolated Hippocampal Neurons through Different Intracellular Mechanisms Amir Paydar '04	61-69
Quantitative Real-Time RT-PCR Assay Shauna Torrence '04	70-81

Cover image: Immunofluorescence of cells transfected with pTRE-ER3C with and without estrogen. By Courtney Frye '05.

An Analysis of the Fibrilization of p53tet-R337H and p53tet-WT

Prentice L. Bowman

St. Jude Supervisor: Richard W. Kriwacki

Faculty Mentor: Terry Hill

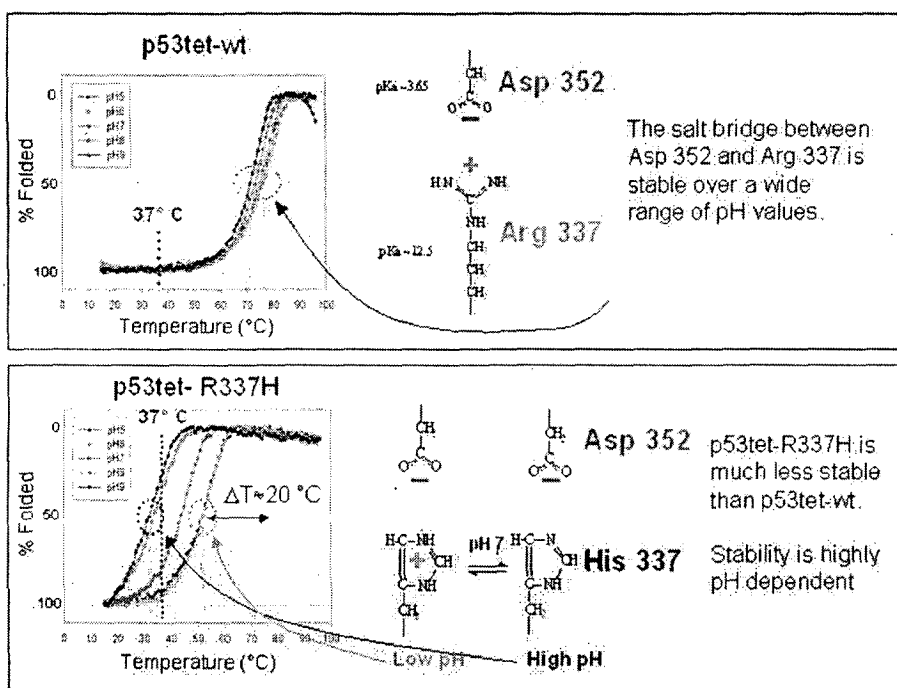
Introduction:

Pediatric Adrenal Cortical Carcinoma (ACC) tumors are very rare as the annual occurrence in the US is about 0.3 per million children under the age of 15. In some areas of Brazil, however, the occurrence of ACC is about 10-15 times greater. Since inherited p53 mutations are associated with the incidence of ACC, researchers examined the coding regions of the p53 genes of 36 patients, and 35 of them displayed a mutation at codon 337 in the tetramerization domain, at which arginine had been replaced by histidine (p53-R337H)¹.

p53 is a tumor suppressor protein that regulates cell growth through apoptosis and cell cycle arrest. As with any protein, the function of p53 is linked to its structure. Alterations in the conformation of the protein inhibit its ability to function, and the result of this is often cancer. However, p53-R337H function is nearly, if not exactly, the same as that of the wildtype (WT)¹. Since there was no apparent change in the function of the protein, the effect of the mutation on the structure and stability of the tetramerization (tet) domain was investigated. It was determined that while p53tet-R337H and p53tet-WT have similar structures, the R337H mutant is less stable. One of the ways in which the domain's stability was tested was by conducting thermal denaturation experiments with the mutant and the wildtype at pHs 5-9 and comparing the results. While p53tet-WT

remains in its normal conformation at all pHs at temperatures up to 50°C, p53tet-R337H begins to unravel at temperatures below 37°C (body temperature). Most importantly, though, the denaturation data also revealed that at pH 5, the WT begins to re-fold itself at high temperatures after being completely denatured². The thermal denaturation results are shown in figure 1 below.

Figure 1:



Another thermal denaturation experiment was then conducted with both versions of p53 at pHs 4-6. At pH 4 after denaturing, both the R337H mutant and the wildtype p53tet fully refolded into a stable, secondary structure that was determined to be fibers².

According to Harper, J.D. and Lansbury P.T., fiber formation consists of three main steps. The first step is a slow nucleation step, in which the protein undergoes unfavorable association steps to form a nucleus or "seed." The second step is a growth phase, in which the nucleus grows rapidly to form polymers. The third step is a steady

state phase, in which the system is at equilibrium and fiber formation is complete³. My research consists of an analysis of the kinetics of p53 fiber formation at pH 4 in an attempt to gain more about the R337H mutant and to see if p53tet fiber formation corresponds with the model illustrated by Harper and Lansbury.

Methods:

The experimental R337H mutant and wildtype p53tet were synthetic. The gene responsible for its transcription was put on a plasmid and transformed into E. Coli for amplification. The p53 protein was then isolated, purified, lyophilized, and placed at -80°C in microfuge tubes for long-term storage. To prepare the protein to be used in the experimental assay, it was dialyzed overnight in the cold room in at least 1L 10 mM NaPi pH 6, 50 mM NaCl. When dialysis was complete, the protein was placed at -20°C for shorter-term storage. When ready to begin the assay, the protein was thawed and diluted to the appropriate concentration(s). Next, 45 ul of 360 mM citrate, pH 3.8 was added to 155 ul of protein to lower the pH to 4, starting the fiber formation process, and the mixture was incubated at the appropriate temperature via a water bath. At time points of 0, 0.5, 1, 2, 4, 6, and 8 hours, 20 ul aliquots were removed from the incubating solution, added to 600 ul of 40 mM NaPi pH 6.0, and placed at 4°C. This action restabilizes the solution, halting fiber formation while maintaining any fibers that may have already formed.

With the use of a fluorometer, the fluorescence of the protein solution was measured at the emission wavelength of 485 nm after 600 ul of the yellow, fluorescent compound Thioflavin T (ThT) was added. The fluorescence of unbound ThT normally peaks near 440 nm, with the fluorescence tapering off at higher and lower wavelengths.

However, when ThT is bound to fibers, its fluorescence peaks near 485 nm. The fluorescence of the entire solution is a composite of the fluorescences of unbound ThT and the bound ThT. Thus, more fibers present in solution means more bound ThT, which causes a higher fluorescence at 485 nm.

The fluorescence of every sample was measured 7 times (every 10 seconds for a minute), and the average of these 7 measurements was used to represent the fluorescence of each individual sample.

Results/Discussion:

The results of the assays were graphed by plotting the fluorescence as a function of the time at which the aliquot was taken. The resulting graphs are as follows:

Figure 2

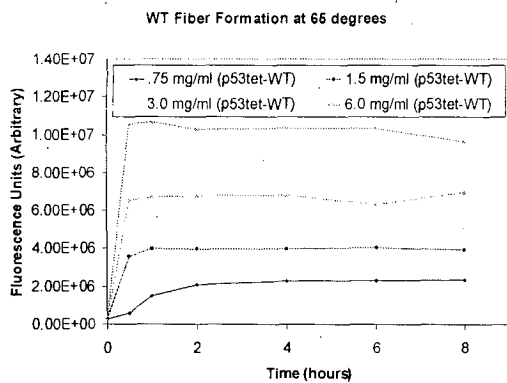


Figure 4

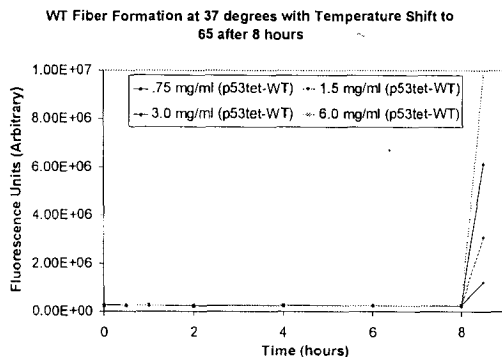


Figure 3

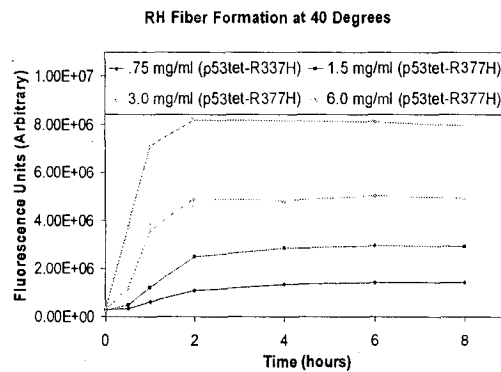
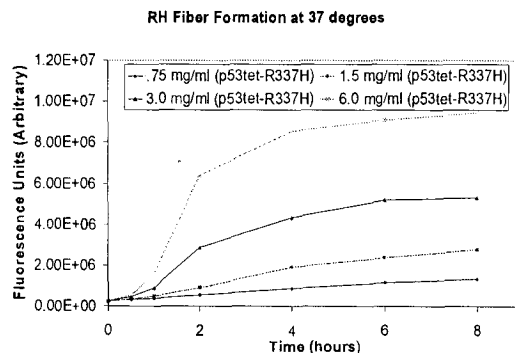


Figure 5



Figures 2 and 4 correspond to wildtype fiber formation at 65°C and 37°C respectively while Figure 3 and 5 correspond to mutant fiber formation at 40°C and 37°C respectively. By comparing figures 2 and 3 or figures 4 and 5, one can see the difference in stability between the wildtype and the mutant. Figures 2 and 3 illustrate complete fiber formation in less than 8 hours. While the mutant does this at 40°C, the wildtype must be placed at a higher temperature in order for this to happen. It should be noted that wildtype does appear reach complete fiber formation about an hour or so before the mutant does, yet these data still show that mutant is less stable than the wildtype. This fact is definitely evident in the comparison between Figure 4 and 5, both of which are at 37°C. At the 8 hour time point, fiber formation is near completion in the mutant, but the wildtype has failed to form any fibers at all. Since the experiment was officially over at the 8 hour time point, the temperature of the water in the wildtype assay was shifted to 65°C as a control to make sure that p53tet protein was actually present in the solution, and the results were positive. Thus, the wildtype appears to be completely stable at 37°C while the mutant is not. Assuming that the *in vitro* effects are the same as the *in vivo* effects, this data suggests that if this mutant form of p53 is subjected to a pH of about 4 in the body, then it will form fibers.

The graphs which “officially” form fibers (figures 2,3, and 5) also show the p53 fiber formation appears to be consistent with the three step model proposed by Lansbury. Furthermore, figures 2 and 3 suggest that the rate of fiber formation is concentration dependent and seems to follow 1st order kinetics (if the concentration is doubled, the rate is doubled. In these figures, fiber formation completes at about the same time at all concentrations. Each concentration differs from the next by a magnitude of two.

Therefore, in order for fiber formation to be complete at the same time at all concentrations, the rates of fiber formation must also differ by a magnitude of two.

Finally, a comparison of Figures 3 and 5 indicates that the rate of fiber formation is also directly related to temperature. The only difference between these two experiments is the temperature at which they were conducted, and fiber formation is slower in the figure corresponding to a lower temperature. However, the direct relationship between rate and temperature may only occur after a certain temperature is reached, one that allows fibers to form. This is suggested by figure 4, in which fibers don't form at all. This failure to form fibers probably occurs because a certain permissive temperature has not been surpassed. If this is the case, then any change in temperature that remains below the permissive temperature would obviously have no effect on the rate of fiber formation because no fibers would form at either temperature.

These results in general imply that the formation and accumulation of stable, non-functional fibers due to the R337H mutation is a major if not the primary cause of ACC. Of course, before this conclusion can be made, more experiments must be conducted, including an investigation to determine if the full-length p53-R337H forms fibers. If the full-length protein forms fibers, then ACC could possibly join the league of diseases known to be linked to the formation of fibers, such as Alzheimer's and Parkinson's disease. These are two of many neurodegenerative disorders characterized by the formation and accumulation of fibers. If it can be determined that ACC is also a result of fibers, then it would probably be able to be treated by creating a drug that increases the stability of p53-R337H, inhibiting the formation of fibers⁴. However, this could only be

done if more is known about the mechanism(s) by which the R337H mutant forms fibers, something that also needs to be studied further.

References:

¹Ribeiro, RC. et al. An inherited p53 mutation that contributes in a tissue-specific manner to pediatric adrenal cortical carcinoma. *Proc Natl Acad Sci U S A.* 98, 9330-5 (2001).

²DiGiammarino EL, Lee AS, Cadwell C, Zhang W, Bothner B, Ribeiro RC, Zambetti G, Kriwacki RW. A novel mechanism of tumorigenesis involving pH-dependent destabilization of a mutant p53 tetramer. *Nat Struct Biol.* 9, 12-6 (2002).

³Harper, JD & Lansbury, PT Jr. Models of Amyloid Seeding In Alzheimer's Disease and Scrapie: Mechanistic Truths and Physiological Consequences of the Time-Dependent Solubility of Amyloid Proteins. *Biochem.* 66, 385-407 (1997).

⁴Koo EH, Lansbury PT Jr, Kelly JW. Amyloid diseases: Abnormal Protein Aggregation in Neurodegeneration. *Proc Natl Acad Sci U S A.* 96, 9989-90 (1999).

Functional analysis of EBNA-3C required for regulation of the EBV oncoprotein LMP-1

Courtney Frye

Professor Loprete

Abstract:

To test the effects of specific protein interaction of the Epstein-Barr virus (EBV) EBNA-3C protein with cellular proteins in its regulation of the EBV oncoprotein LMP-1, modified EBNA-3C genes were cloned into the pTRE vector, which contains a Tetracycline responsive minimal CMV promoter (P_{minCMV}). The specific plasmids used encoded a Flag tag wild-type EBNA-3C, a Flag tagged EBNA-3C with the amino acids 629-683 deleted, and an EBNA-3C fused N-terminal to an estrogen receptor (ER). Each gene was cloned downstream of the P_{minCMV} , which allows for the regulation of EBNA-3C expression in mammalian cells through the chemical doxycycline. These plasmids were then used to develop a Double-Stable BD Tet-Off cell line in Raji cells. Through PCR (Polymerase Chain Reaction) and Western Blot analysis, this process selected individual cell lines with high EBNA-3C expression in the absence of doxycycline and a lack of EBNA-3C expression in the presence of doxycycline. Selected cell lines can then be used to explore the specific effects of EBNA-3C on the expression of LMP-1.

Introduction:

The Epstein-Barr virus (EBV), which is commonly transmitted through saliva, has a virion structure like that of all herpesviruses and is a member of the Herpesviridae family. Initial exposure to EBV, which occurs primarily during childhood, may lead to an asymptomatic primary infection or a symptomatic infection such as infectious mononucleosis (IM). IM, an immune response to the virus, presents with non-specific symptoms of an upper respiratory infection. (Miller 1990). Primary infection establishes a latent infection in B lymphocytes (B

cells) that, once established, will maintain itself for the remainder of life. The exact method of establishment of latent infection is currently under debated. It is thought that direct infection of B cells of the oropharyngeal cavity or replication in epithelial cells which secondarily infect circulating B cells is the primary method of infection. (Kieff & Rickinson, 2003; Zhao & Sample, 2000; Sample, 1999).

EBV's main activity is its ability to cause open-ended *in vitro* proliferation of B cells or immortalization. Immortalization is a two stage process consisting of a preliminary phase of B cell activation in which the virus binds to the cell surface, and a secondary stage of unending blastogenesis which necessitates the production of EBV gene products. (Miller 1990). EBV has oncogenic properties and is associated with malignancies such as nasopharyngeal carcinoma, Burkitt's lymphoma, and Hodgkin's disease, among many others. EBV latency has been studied *in vitro* using EBV-immortalized B lymphoblastic cell lines (LCLs) and Burkitt's lymphoma (BL) cell lines. These cells express latency-associated genes (12 EBV genes) including 6 EBV nuclear antigens (EBNA-1, -2, -3A, -3B, -3C and -LP) and 3 latent membrane proteins (LMP-1, -2A and -2B). Of the 12 EBV genes, six, including EBNA-3C and LMP-1, are required for B cell immortalization. EBNA-3C and LMP-1 are also extremely influential in the control of cell differentiation and growth due to their effect on cellular signaling pathways. EBNA-3C has been shown to activate expression of the oncogenic LMP-1 protein, which is not capable of sustaining B cell growth alone but is largely involved with cell survival and proliferation. A number of associations between EBNA-3C and cellular proteins, many of which are transcription factors, have been reported, but it is not known which of these are required for activation of LMP-1. (Kieff & Rickinson, 2003; Zhao & Sample, 2000; Sample, 1999).

The human Burkitt lymphoma cell line Raji posses EBV DNA that has two deletions, one of which results in the deletion of EBNA-3C while the remaining latent genes are still able to be expressed (Polack *et al.*, 1984). Therefore, EBNA-3C can be introduced into Raji cells and the specific effects due to EBNA-3C can be observed. The pTRE vector is a response plasmid that has a Tetracycline responsive element (TRE) just upstream of a minimal CMV promoter (P_{minCMV}), which allows for control of genes cloned downstream of the promoter. The TRE responds to a tetracycline-controlled transactivator (tTA), a chimeric protein, which is constitutively expressed from the pTet-Off regulator plasmid. The tTA binds the TRE and activates transcription in the absence of doxycycline (EBNA-3C gene expression) or presence of doxycycline (no EBNA-3C gene expression). Cells influenced by this specific mechanism are referred to as Tet-Off cells. Raji cells can also be transfected with a pJ6 Ω puro plasmid in conjunction with the pTRE plasmid to allow for selection by puromycin resistance. (BD Tet User Manual, 2002). Induction of wild-type EBNA-3C expression leads to an increase in LMP-1 expression and a dramatic phenotypic change in the cells (Sample, Unpublished).

The objective of this research was to determine which domains of EBNA-3C are required and thus, which of the interactions between the EBNA-3C protein and cellular proteins are essential for regulation of the LMP-1 protein. This project focused specifically on acquiring the tools necessary to distinguishing the effects of different domains of EBNA-3C in regard to regulation of LMP-1 and cellular transcription factors. This was to be accomplished through the establishment of multiple double-stable Tet-Off cell lines.

Methods:

In order to study the specific effects of the EBNA-3C protein, an array of 11 different EBNA-3C genes were produced (Figure 1). This includes the EBNA-3C wild-type genes tagged

with the Flag epitope, different EBNA-3C mutant genes, and an EBNA-3C gene fused to the estrogen receptor (ER). The 11 EBNA-3C variations were cloned into separate pTRE response plasmids downstream of the P_{minCMV} . Using the pTRE EBNA-3C genes, FuGENE transfections were performed to check for protein expression of each pTRE EBNA-3C genes.

First, 293T adherent cells were plated in a six-well plate at 1.5×10^5 cells per mL with 2 mL in each well. The cells were incubate overnight in order to reach 50-70% confluency for the transfection. The follow day, Eppendorf tubes were set up and properly labeled in the tissue culture hood where the transfection was to take place. Via pipet, 92 μl of serum-free DMEM media, 6 μl of FuGENE 6 Transfection Reagent (Roche Diagnostics Corporation), 1 μl of the appropriate pTRE EBNA-3C gene, and 1 μl of the pTet-Off regulatory plasmid were added to each Eppendorf. After incubating for 15 minutes at room temperature, the contents of each Eppendorf were added to one of the 6 wells by pipet and then mixed by swirling the entire plate. The plate was then incubated for 48 hours to allow the transfection to occur. After 48 hours, the media was aspirated from each of the 6 wells. 1 mL of PBS (1x) was carefully added to each well, swirled around, and then aspirated off. The process of adding and aspirating PBS for each well was repeated a second time. 500 μl of SDS Cracking Buffer (2x) was used to resuspend and transfer the sample from each well to the appropriately labeled Eppendorf tube. Each sample was sonicated for 10 seconds at 40 on the output control to lysis the cells. The sonication process was repeated two more times for a total of 3 sonications per sample.

50 μl of SDS Sample Buffer (1x) was added to each sample before being boiled for 2 minutes and centrifuged for 5 minutes at 10,000 RPM. 20 μl of each sample was run on a 8.5% SDS Page gel (2x) and transferred to Immobilon-P membrane by Western Blotting. One membrane, entitled Flag, was probed by the Anti-Flag M2 monoclonal antibody (Sigma) in a

1:10,000 dilution. Later, it was probed with a secondary antibody of Anti-Mouse Ig (Amersham Biosciences UK limited) in a 1:25,000 dilution. The second membrane, called 3C, was probed with a polyclonal 3C primary antibody in a 1:50:000 dilution and a Rabbit x Sheep secondary (Chemicon International) in a 1:25,000 dilution. The Flag membrane was treated with the ECL Western Blotting Kit and applied to Hyperfilm for 40 seconds and 2 minutes with adjustments being made for background. The 3C membrane, however, expresses better with the use of the ECL +Plus Western Blotting Kit. The 3C membrane was exposed to Hyperfilm for 10 seconds and 2 minutes with adjustments in time being made for clarity. The visualization of bands of correct sizes at specific locations indicates the successful expression of the EBNA-3C genes from the pTRE plasmids.

Successful plasmids were used to develop multiple double-stable Tet-Off cell lines in Raji cells. First, 8.0×10^6 cells per sample were centrifuged for 5 minutes at 1,000 RPM. For each sample to be transfected, a T-25 tissue culture flask was properly labeled. 1 mL of the supernatant was pipetted into each flask along with 9 mL of the Tet-Off media (See Procedure). The remainder of the supernatant was aspirated and the pellet was resuspended in 250 μ l of Tet-Off media per sample. 250 μ l of resuspended cells were pipetted into each properly labeled cuvette along with 15 μ l of the appropriate pTRE expression plasmid. 1 μ l of the pJ6 Ω puro plasmid, which allows for selection of cells based on puromycin resistance, was also added to each cuvette. The samples were incubated for 10 minutes at room temperature before being electroporated at 250 V and 960 μ F. The samples were incubated on ice for 10 minutes before being resuspended in 700 μ l of cold PBS and being transferred to the corresponding T-25 flasks. Doxycycline, the chemical that regulates gene expression, was added to each flask to achieve a final concentration of 1 μ l / mL. (BD Tet User Manual, 2002)

The cells were grown for 2 days before being plated into 24 well-plates at a concentration of 1 to 2×10^3 cells per well. The cells were diluted to the proper concentration using the Tet-Off media with freshly added doxycycline (see above concentration). Over the course of 2-4 weeks, the cells were feed at least weekly with the Tet-Off media (with doxyclyine added) and evaluated using a microscope to find isolated, healthy colonies. Those cells demonstrating puromycin selection were plated into six-well plates and later split into small flasks if they continued to grow healthily. Samples from these flasks were frozen in liquid Nitrogen for later use. (BD Tet User Manual, 2002)

To determine the success of our double-stable Tet-Off Raji cell lines, a Qiagen DNA extraction was performed on samples from the aforementioned T-25 flasks. First, 5 mL of 1×10^6 cells per mL of each sample were aliquoted into individual Eppendorfs and centrifuged for 5 minutes at 400 RPM. The supernatant was aspirated off taking great care not to disturb the pellet. Each pellet was resuspended in 20 μ l Proteinase K (from kit) before the addition of 200 μ l Buffer AL (from kit). Each sample was pulse vortexed for 15 seconds and then incubated at 56°C for 10 minutes. 200 μ l of ethanol (96-100 %) was added to each sample, which was then pulse vortexed for 15 seconds. The QIAGEN spin columns were labeled and placed in collection tubes and the Eppendorf contents were transferred to the correspondingly labeled spin columns. Each sample was centrifuged for 1 minute at 8,000 RPM, and then the collection tube was discarded and replaced by an empty collection tube. 500 μ l of Buffer AW1 (from kit) was added to each sample and the same centrifuge and collection tube procedure was repeated (see previous step). 500 μ l of Buffer AW2 (from kit) was added to each sample, which were then centrifuged for 3 minutes at 14,000 RPM. The collection tubes were replaced and the samples were centrifuged again for 1 minute in an optional step to prevent DNA contamination. The collection

tubes were discarded and replaced by Eppendorfs before the addition of 200 μ l of Buffer AE (from kit) and incubation at room temperature for 1 minute. The samples were centrifuged at 8,000 RPM for 1 minute, which concluded the DNA purification process. (Qiagen, 1999).

Samples from the previous DNA extraction were then used in a Polymerase Chain Reaction procedure to screen clones for the presence of the EBNA-3C vector. This was accomplished by selecting a portion of the ENBA-3C vector that was common to all of the genes, Δ 690-750, creating primers to amplify this portion of the protein, and creating a PCR program with the temperatures and time frames best suited for amplification of this specific portion.

	<u>F-3C Primers</u>
F-3C Screen Fwd	CCCACGGGCTCCAATCATCTTCA
F-3C Screen Rvs	GGGAATCTTGTTGGAATGGGGCG
	<u>PCR Program</u>
	94°C for 5 minutes—Hold
	<u>8 Cycles</u>
	95°C for 20 seconds
	66°C for 20 seconds
	72°C for 30 seconds
	<u>35 Cycles</u>
	95°C for 20 seconds
	62°C for 20 seconds
	72°C for 30 seconds
	72°C for 7 minutes—Hold
	4°C until end

Properly labeled PCR mini-tubes were setup for each sample purified above, a negative control, and a positive control. 1 μ l of both Fwd and Rvs Primers (10 mM), 1 μ l dNTPs (10 nM), 5 μ l Tag 10x Buffer, and 0.75 μ l Tag Expanol (5 units / 1 μ l) were added to each tube. 1 μ l purified DNA and 50 μ l DDH₂O were added to each tube except the negative control (positive control F-3C purified DNA). No purified DNA was added to the negative control so 51 μ l DDH₂O was added to maintain the same volume in all the sample tubes. The tubes were randomly distributed across the holding grid of the GeneAmp PCR System 9700 (PE Applied

Biosystems) and the above program was activated. Several hours later, the samples were run on an agarose gel to confirm the presence of EBNA-3C vector in the Raji cells. The visualization of bands running at the same size, 340 base pairs, is an affirmation of the presence of the EBNA-3C vector.

The Estrogen Receptor (ER3C) plasmid, when found in cells, is retained in an inactive state in the cytoplasm of the cell. ER3C should only become active and move into the nucleus if it comes into contact with the hormone estrogen. To test the ability to regulate this process, pTRE ER3C was FuGene transfected into 293T cells (see previous procedure). The samples were allowed to grow for several days and then split onto two slides. The cells of one slide were fed with media containing estrogen and the other cells were fed with media lacking estrogen. Both slides were then treated with a primary antibody, α - ER Rabbit diluted 1:200 in PBST + rabbit serum, and a secondary antibody, α - Rabbit which fluoresces diluted 1:200 in a PBST + rabbit serum which fluoresces. Under appropriate conditions, this sequence of antibodies allows the location of the pTRE ER3C to be visualized. The two slides were examined by immunofluorescence microscopy to verify that cells treated with estrogen would contain ER3C in the nucleus and that cells lacking estrogen would contain ER3C in the cytoplasm.

Results and Discussion:

To verify that the pTRE EBNA-3C plasmids could be expressed and produce proteins of the appropriate size, plasmids were transfected into 293T cells using a FuGene transfection. The results for the western transfer probed with the anti-Flag antibody (Figure 2) show detection of proteins at the predicted sizes from each EBNA-3C gene. The visualization of bands of correct sizes relative to the specific sample confirms expression of the plasmid. The positive controls in lanes 1 and 2 ran at the appropriate sizes. Lane 3 was blank as was expected for the negative

control. In lane 4, the wild-type Flag-EBNA-3C (F-3C) sample ran the same size as the positive control in lane 1, which was from a previously confirmed F-3C sample. Lane 5 is blank as was expected because the ER3C sample did not have a Flag tag and is therefore unable to be detected by this antibody. The Flag-EBNA-3C Δ 629-683 (F-3C Δ 629-683) has a deletion that makes it slightly smaller than the original F-3C, consequently F-3C Δ 629-683 was expected to run a little faster (lower on the gel) than F-3C. While the difference between the F-3C and the F-3C Δ 629-683 is not great, the F-3C Δ 629-683 does appear to have run a little lower.

The results for the western transfer analyzed with anti-EBNA-3C antibodies were similar (Figure 3A). Lanes 1 and 2 contain the positive controls F-3C and F-3C Δ 11-365 respectively, which ran at the appropriate sizes. Lane 3 is blank because protein ladders show up on transfers but not on film, and lane 5 is blank because it is a negative control. F-3C and F-3C Δ 629-683 in lanes 4 and 6 respectively, ran at the appropriate sizes with F-3C Δ 629-683 running slightly lower than F-3C. While ER3C should have been detected by the anti-3C in lane 7, it is not present at this exposure time. A longer exposure time, Figure 3B revealed a faint ER3C band running at a larger molecular weight (higher on the gel) than the other samples as was expected due to its large size.

The PCR procedure amplified a region of DNA, Δ 690-750, within the EBNA-3C gene which is common to all the modified pTRE EBNA-3C plasmids. Therefore, the PCR results from the double stable Raji cell line samples containing the EBNA-3C modified plasmids should all yield a fragment migrating at the same size, 340 base pairs. Initial data shown in Figure 4 demonstrates (excluding lanes 1, 16, 17 as markers and lane 14 as a negative control) that almost all the samples produced a band that ran at the correct size and therefore contained the EBNA-3C gene. Lane 5, also a negative control, contained a weak band suggesting a small amount of

contamination. Lane 8 also showed a very weak band. Since one of our two negative controls revealed a band, we cannot determine whether the weak band in lane 8 reflects the presence of the plasmid in the cells, or is the result of additional DNA contamination. Due to the possibility of contamination, probably from the use of non-filter tips, the PCR will be repeated and the gel will be rerun. Although there appears to be some contamination, the strong bands produced for several samples are a good indication of the successful production of double-stable transfected Raji cell lines.

The immunofluorescence of ER3C demonstrates our ability to regulate the activation of ER3C, and as such directly influence the activities of the nucleus of a cell. Figure 5 A, clearly shows that the 293T cells treated with the media lacking estrogen contained ER3C in the cytoplasm of the cell (the bright area surrounding the dark nucleus). Figure 5 B, shows that cells treated with media including estrogen contained ER3C in the nucleus of the cell (the bright area or bright spots surrounded by the dark cytoplasm).

The newly established Tet-Off Raji cell lines can now be utilized in further exploration of determining which domains of EBNA-3C are required for interaction with cellular proteins for regulation of the oncogenic LMP-1 protein.

References:

- BD Tet-Off and BD Tet-On Gene Expression Systems User Manual. Cat. No. K1620-1 & K1621-1. 2002. BD Biosciences Clontech.
- Kieff, E. & Rickinson, A. B. (2003). Epstein-Barr Virus and Its Replication. pp. 2511 - 2573.
- Miller, George. (1990). Epstein-Barr Virus: Biology, Pathogenesis, and Medical Aspects. In: Fields BN, Knipe DM, *et al* (eds) *Virology*, 2nd edn, pp. 1921-1957. New York: Raven Press Ltd.
- Polack, A., Delius, H., Zimmer, U., & Bornkamm, G. W. (1984). Two deletions in the Epstein-Barr virus genome of the Burkitt lymphoma nonproducer line Raji. *Virology*, pp. 133, 146-157.
- QIAGEN. QIAamp DNA Mini Kit and QIAamp DNA Blood Mini Kit Handbook. (1999).
- Sample J, Sample C. (1999). Epstein-Barr virus: Molecular biology. In: Webster RG, Granoff A, eds. *Encyclopedia of virology*, second edition. London: Academic Press, pp 494-501.
- Zhao, B. & Sample, C. E. (2000). Epstein-Barr virus nuclear antigen 3C activates the latent membrane protein 1 promoter in the presence of Epstein-Barr virus nuclear antigen 2 through sequences encompassing an Spi-1/Spi-B binding site. *J. Virol.* pp. 74, 5151-5160.
- Zhou Z, Prasad B, Jakana J, Rixon F, Chiu W. (1994). Protein subunit structures in the herpes simplex virus A-capsid determined from 400 kV spot-scan electron cryomicroscopy. In: *Journal of Molecular Biology*, pp. 242, 456 -469.

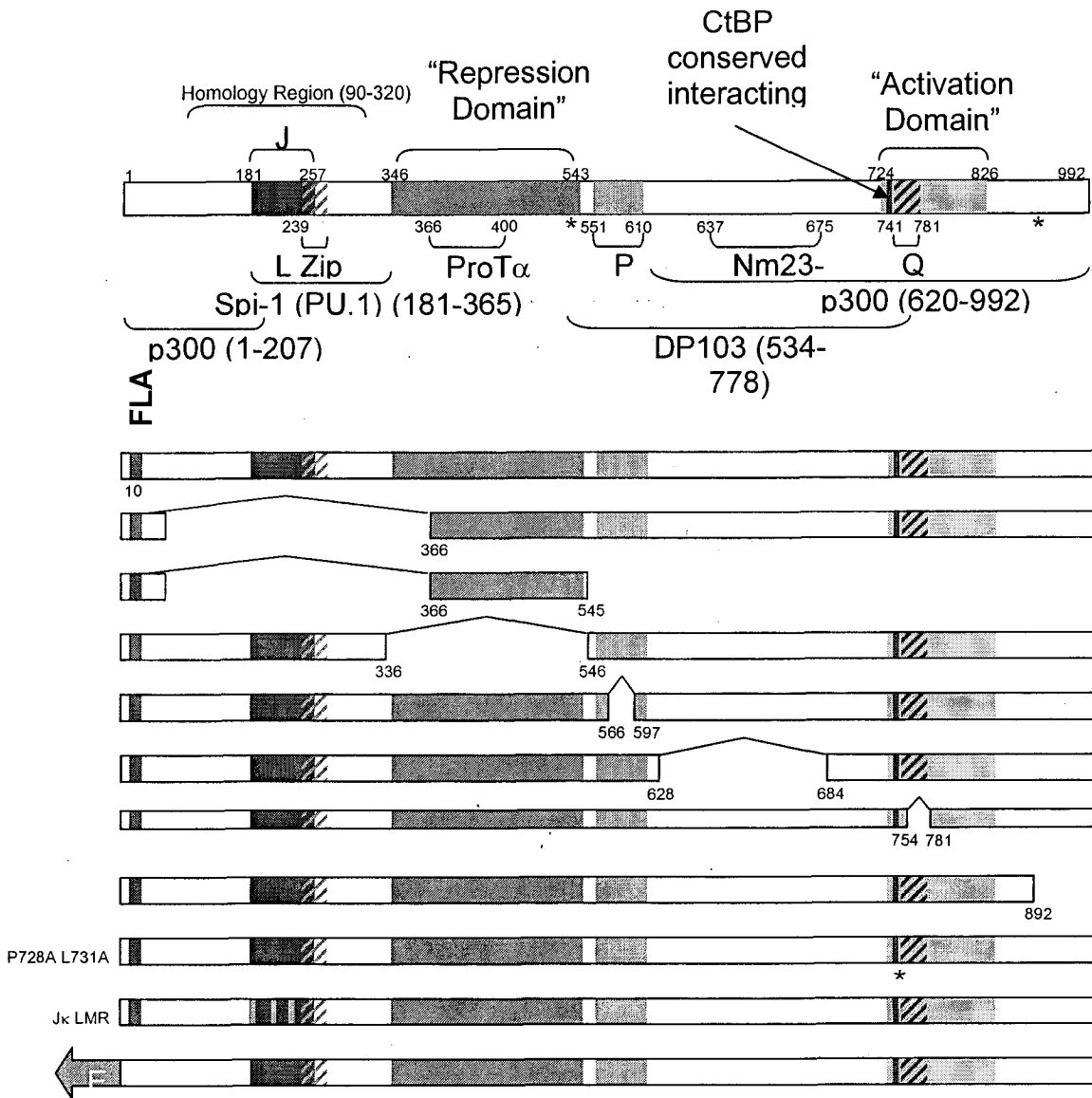


Figure 1: EBNA-3C Constructs

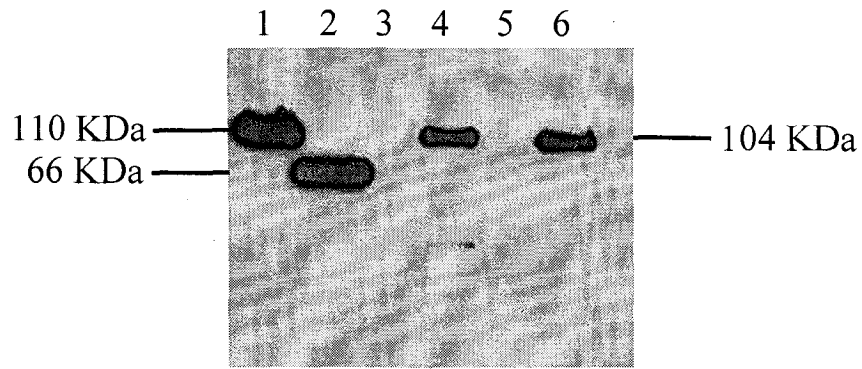


Figure 2.
Western transfer of EBNA-3C
expression in 293Ts with anti-FLAG
M2.

Lane 1—F-3C Full Length

Lane 2—F-3C Δ 11-365

Lane 3—(-) Control

Lane 4—F-3C

Lane 5—ER3C

Lane 6—F-3C Δ 629-683

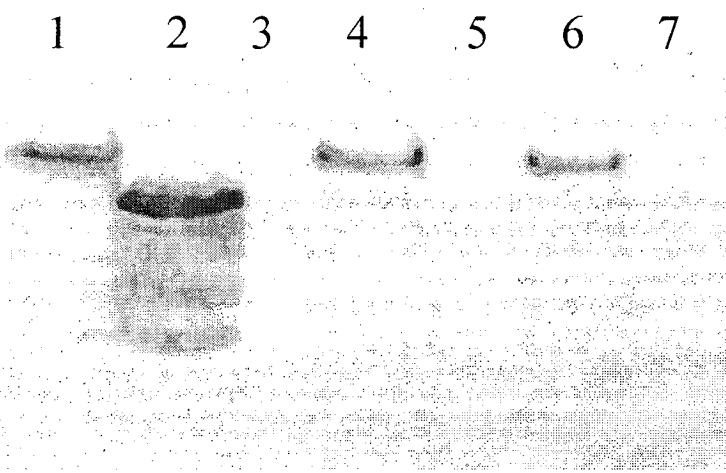


Figure 3 A.
Western transfer of EBNA-3C expression in
293Ts with anti-3C .
Lane 1—F-3C
Lane 2—F-3C Δ 11-365
Lane 3—Protein Ladder
Lane 4—F-3C
Lane 5— (-) Control
Lane 6—F-C3 Δ 629-683
Lane 7—ER3C

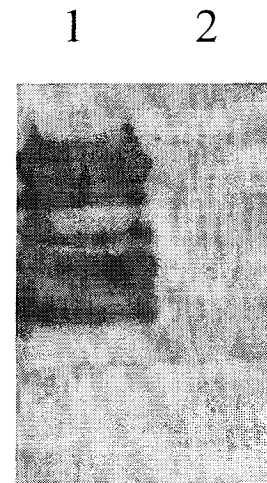


Figure 3 B.
Longer exposure of
anti-3C western.

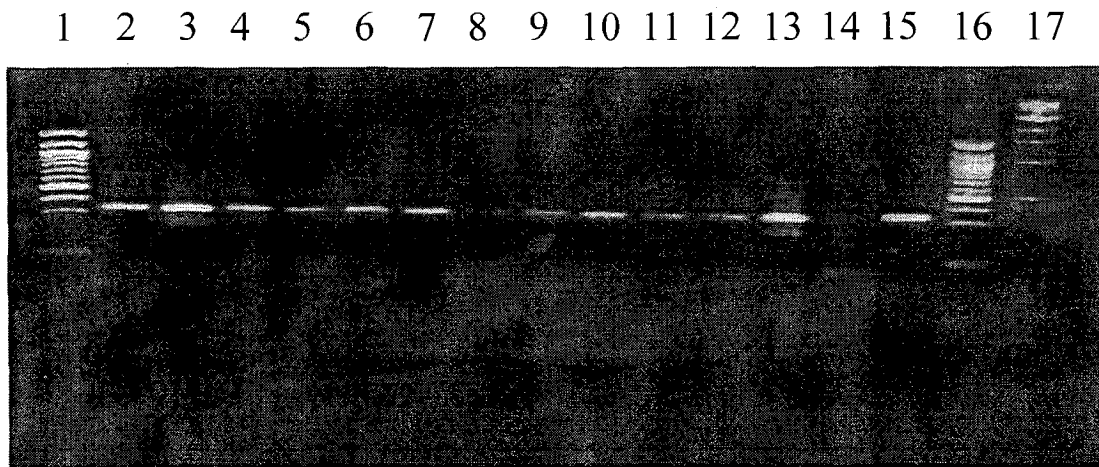


Figure 4
An agarose gel of EBNA-3C PCR samples.

- | | |
|------------------------------------|-------------------------------------|
| Lane 1— 100 Kb Ladder | Lane 10—ER3C (S 11) |
| Lane 2— F-3C (S 6) | Lane 11—F-3C Δ 629-683 (S 4) |
| Lane 3—F-3C Δ 629-683 (S 3) | Lane 12—F-3C (S 7) |
| Lane 4—F-3C Δ 629-683 (S 1) | Lane 13—F-3C (+) Control |
| Lane 5—(-) Control | Lane 14—F-3C (Confirmed +) |
| Lane 6—F-3C Δ 629-683 (S 2) | Lane 15—(-) Control |
| Lane 7—ER3C (S 12) | Lane 16—100 Kb Ladder |
| Lane 8—ER3C (S 10) | Lane 17—1 Kb Ladder |
| Lane 9—F-3C (S 8) | |

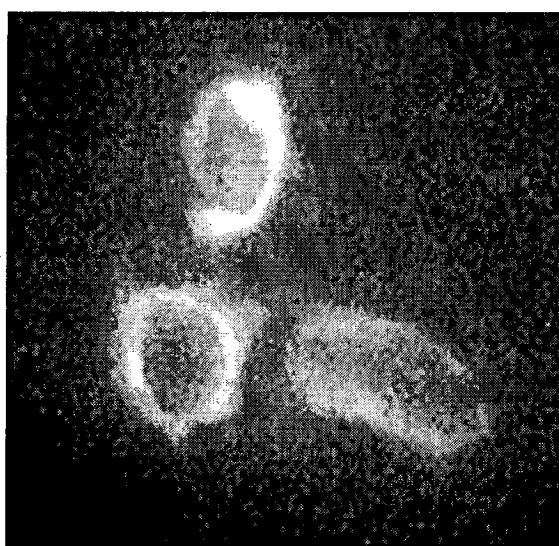


Figure 5 A.

Immunofluorescence of cells transfected with pTRE-ER3C without estrogen. The protein is in the cytoplasm (dark is nucleus).

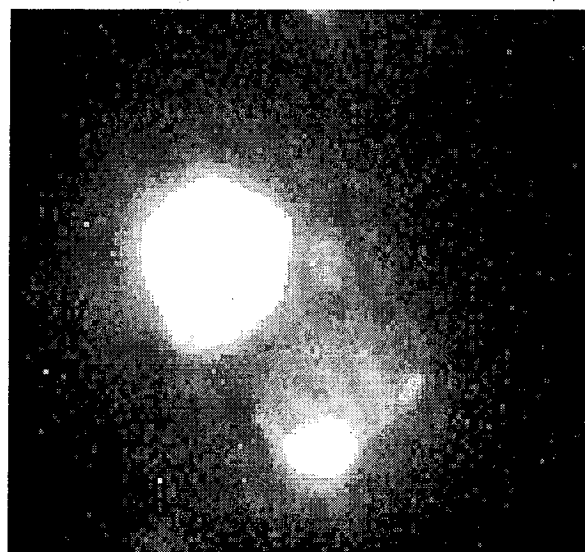


Figure 5 B.

Immunofluorescence of cells transfected with pTRE-ER3C with estrogen. The protein is in the nucleus; sometimes all over or in spots (lower cell).

Investigation into the Herpes Simplex Virus Type 1

Alison Groeger

A. Herpes Simplex Virus Type 1 as the Cause of Cold Sores

Herpes simplex virus type 1, HSV-1, is a virus that causes small red lesions commonly known as cold sores or fever blisters. Between 60% and 95+% of people in various populations are infected with HSV-1, but only about a third of those infected develop lesions (5, 37).

Approximately nine out of ten Americans become infected with HSV-1 during their lifetime (5). HSV-1 lesions commonly appear on the lips or other oral tissues, but the virus has been known to show symptoms in ocular tissue, genital tissue, and to a lesser extent, other human and mammalian tissues (see figure 1). The virus usually spreads from individuals shedding the virus sharing food or kissing others. Since only one third of those infected express visible symptoms, a person can spread the virus unknowingly during periods of viral shedding (5).

Once infected with HSV-1 a person will carry the virus for life. HSV-1 has the ability to establish latency in sensory neurons and the neurons of the central nervous system, in particular aural neurons. During HSV-1 latency, viral DNA exists in the nuclei of ganglia as extrachromosomal concatemers (15). Latency permits recurrent infections during periods of stress, such as lack of sleep, exposure to ultra violet radiation, and weakened immune system. Primary infection with HSV-1 usually causes "mild flu-like symptoms," which include soreness and swelling in the mouth, swollen lymph nodes in the neck, and fever. Those who develop lesions do so upon recurrent infections, during which a cluster of small blisters turn into painful sores, crust over, and eventually heal. These infections usually last seven to fourteen days (5).

To those with normal immune systems, oral HSV-1 infections are not serious. However, physicians can prescribe topical creams, such as Zovirax® (acyclovir) and Denavir® (penciclovir), to reduce pain and duration of problematic infections (5).

B. Classification and Architecture of Herpes Simplex Virus Type 1

Herpesvirus Subfamily	Common Name	Scientific Name	Diseases Caused
Alpha herpesviruses: •Neurotropic (infect nervous system tissue) •Short reproductive cycle •Efficient cell destruction •Variable host range	Herpes simplex virus 1	Human herpesvirus 1	Facial, labial and ocular lesions
	Herpes simplex virus 2	Human herpesvirus 2	Genital lesions
	Varicella zoster virus	Human herpesvirus 3	Smallpox, chickenpox, shingles
Beta herpesviruses: •Lymphotropic •Long reproductive cycle •Enlargement of infected cells •Limited host range	Human cytomegalovirus	Human herpesvirus 5	Birth Defects
	No common name	Human herpesvirus 6 and 7	Mild early childhood roseola
Gamma herpesviruses: •Lymphotropic (specifically T or B lymphocytes) •Latency observed in lymphoid tissue	Epstein-Barr virus	Human herpesvirus 4	Infectious mononucleosis
	Karposi's sarcoma herpesvirus	Human herpesvirus 8	cofactor in Karposi's sarcoma

Table 1: Table classifying the eight different types of human Herpesviruses (18, 36).

HSV-1 is one of the many members of the *Herpesviridae* family. This family demonstrates great diversity in host range, as well as conservation of 26 genes among the three subfamilies (15, 42). Not only do herpesviruses infect a variety of vertebrates and a few species of invertebrates, the three subfamilies, Alpha herpesviruses, Beta herpesviruses, and Gamma herpesviruses, can infect a variety tissues. There are eight members of the *Herpesviridae* family that are known to infect humans (see Table 1). Herpes simplex-1 is an Alpha herpesvirus because of its short reproductive cycle, ability to infect nervous tissues, lytic cycle, and wide host

range including a variety of small mammals such as mice, guinea pigs, and rabbits. This wide host range makes HSV-1 a convenient virus to study *in vivo*.

Viruses belonging to the *Herpesviridae* family usually share four major characteristics; (1) herpesviruses encode a variety of enzymes that promote virus replication, (2) viral capsids and the viral genome are synthesized in the nucleus, (3) herpesviruses eventually destroy host cells, (4) most herpesviruses have the ability to “remain latent in natural hosts”(37). All herpesvirions have a core composed of viral DNA, a capsid, a tegument, and an envelope (see Figure 2) (37).

A herpesvirus core is composed of a single linear double-stranded DNA molecule “packaged in the form of a torus” (37). The viral capsid or nucleocapsid surrounding the core (see Figures 3 and 4) is approximately 15 nm thick and 100 nm in diameter (6, 15). It is an icosahedral structure composed of six different types of protein, with a triangulation number of $T=16$ (6, 15, 36, 37, 45, 47). It is constructed of 12 pentameric and 150 hexameric capsomeres, for a total of 162 capsomeres (6, 15, 36, 45, 47). Capsomeres are connected by trivalent structures called triplexes (6).

Surrounding the capsid is a protein layer of variable structure called the tegument (see figure 2) (37). The tegument is composed 15-20 proteins. Two of these tegument proteins, VP16 and vhs, enhance viral gene expression in addition to supporting virion structure (47). The envelope is an altered host cell membrane encasing the tegument and bears at least 11 viral glycoproteins, appearing as “short spikes embedded in the envelope” (see Figure 2)(36, 37). Finally, the entire HSV-1 virion is approximately 200 nm in diameter (6).

C. Description of HSV-1 lytic cycle

The length of the HSV-1 lytic cycle is approximately eighteen hours from infection to lysis. Viral infection of a target cell begins with the binding of glycoprotein-C (gC), one of many glycoproteins embedded in the viral envelope, to cellular membrane proteoglycans, such as heparan-sulfate (see Figure 5). Once the virus has attached to the target cell membrane, gD binds to cellular HVEM (herpesvirus entry mediator) receptors and gB and other viral glycoproteins prompt the fusion of the two membranes (37, 47). Fusion of the viral envelope with the host cell's plasma membrane releases viral contents into the cytoplasm. Upon release, members of the tegument, begin to prepare cellular machinery for virion production. One of these members, the virus host shutoff protein, vhs, begins to destroy mRNA and degrade polysomes. Other members of the tegument such as VP16 (see α -TIF in Figure 5) are transported to the nucleus where they promote transcription of viral genes.

The capsid and associated proteins are also released upon fusion and transported to the surface of the nuclear envelope by microtubules and cellular transport machinery (37, 47). Subsequently, capsid proteins associate with nuclear pore complexes in the nuclear envelope and promote the injection of viral DNA through the nuclear pore into the nucleus (see Figure 5) (37, 47). Once in the nucleus, viral DNA circularizes with the help of nuclear and viral proteins, and uses cellular RNA polymerase II to transcribe mRNA. HSV genes are expressed in a regulatory cascade, beginning with Immediate Early (IE) or α genes, followed by Early (E) or β genes, and finally Late (L) or γ genes (see Figure 7). The HSV genome is approximately 152 kbp in length and encodes over 80 proteins (6, 15, 37, 47). The six major regions of the HSV-1 genome are the ends, the long repeat (R_L), the long unique region (U_L), the short repeats (R_S), the origins of replication, and the unique short region (U_S) (See Figure 6). The ends of the viral DNA are important for circularizing linear DNA upon entry into the nucleus and packaging DNA in the

virion (47). U_L and U_S regions and contain at least 56 and 12 ORFs respectively and encode for the majority of viral proteins. The pairs of inverted repeats bind the U_L and U_S regions in addition to encoding for important IE regulatory proteins and latency genes.

Although the regulatory cascade is divided into three basic phases of gene expression (IE, E, L), the actual expression process is more of a continuous cascade with certain genes reaching peak transcription rates before others in the same phase. VP16 aids in initiating transcription of the 6 IE genes. IE protein synthesis peaks at about 2-4 hours after a cell has been infected, but some IE proteins will continue to be synthesized through the rest of the cycle (15, 37). Once synthesized, 5 of the six IE proteins enter the nucleus to participate in transactivation of E genes. E genes encode for enzymes that assist in viral gene regulation, nucleotide metabolism, and the replication of viral DNA. Synthesis of E protein experiences peak rates between 4-8 hours postinfection, and DNA replication begins between IE and I protein synthesis and continues for 12 hours (15, 37). E proteins include thymidine kinase, ribonucleotide reductase, viral DNA polymerase, viral proteins with helicase and primase activities, and a protein involved in DNA replication and gene regulation called ICP8. E proteins induce the transcription of L genes, which code for capsid proteins, tegument proteins, and viral glycoproteins. L genes peak expression at various times during or after viral DNA synthesis (15, 37, 47).

Before the synthesis of capsid proteins, E proteins replicated nicked viral DNA via a rolling circle mechanism to produce DNA concatemers (37). Subsequently, capsid proteins, produced in the L phase of expression, localize to the nucleus where the viral capsid is assembled. Assembly begins with the construction of a capsid scaffold, to create a procapsid. Then portions of a concatemer are cleaved into monomers after being inserted into the procapsid. With capsid proteins and DNA in place, degradation of scaffold proteins ensues. The complete

capsid then buds through the inner nuclear membrane containing viral glycoproteins. After release into the cytoplasm, capsids associate with viral tegument proteins (including VP16 and vhs), and bud into exocytotic vesicles containing viral glycoproteins. Mature virions then bud from the cell membrane and go on to infect other cells (15, 37, 47).

D. Details on VP16

The herpes simplex virus type 1 exploits cellular resources and machinery to produce more virions. Virus particle 16, VP16, is a prime example of this ability to utilize the host cell's natural processes for viral production. The VP16 phosphoprotein is also known as alphaTIF (alpha trans-inducing factor), Vmw65, and ICP25. Its location on the HSV-1 genome is U_L48, and it does not demonstrate differential expression. VP16 is a structural member of the HSV-1 virion tegument that enters the nucleus with viral DNA. In addition to its role as a *trans*-activator of genes, VP16 also modulates the viral host shutoff protein, vhs, and recruits vhs to nascent virion capsids in the cytoplasm (40).

Upon infection, VP16 is released from the viral envelope into the cytoplasm where it dissociates from its partner tegument protein, vhs, and binds to host cell factor 1, HCF. VP16 is believed to have a higher binding affinity for HCF than vhs and forms a DNA-independent heterodimeric complex. HCF then escorts VP16 proteins to the nucleus where the two form a complex with Oct-1 and DNA (see Figure 8) (21, 23, 30, 53). Once in the nucleus, VP16 directs the formation of a multiprotein-DNA complex (see Figure 9) (4). VP16 is a powerful transactivator, which acts upon the cis-regulatory elements located in the promoter sequences of the immediate-early (IE) genes. However, VP16 has weak DNA-binding affinity when it is not bound as part of the VP16 induced complex, VIC (13, 40). This complex includes two host cell

transcription factors, Oct-1 and HCF-1, and viral DNA coding for the cis-regulatory sequence TAATGARAT (where R is a purine).

Oct-1 is an octamer-binding transcription factor with a POU domain allowing Oct-1 to bind to ATGCTAAT consensus sequences. The POU domain has two regions; a carboxy-terminal POU homeodomain (responsible for binding to DNA) and an amino-terminal POU-specific sub-domain linked by a flexible sequence of amino acids (4). Studies have also demonstrated that VP16 binds to two specific sequences in the cis-regulatory elements of IE genes (2, 30, 35, 38). The GARAT sequence is important for VP16 binding to DNA in the VIC complex, as well as the 3-bp D element, located 3' of the GARAT sequence (4). At low multiplicities of infection, MOI, VP16 is required for initiating viral gene transcription (2, 44). However, once immediate early gene transcription has begun, the expression of these genes is enough to sustain the lytic cycle.

VP16 also regulates gene expression by binding to and deactivating the virion host shutoff protein, vhs (see Figure 9) (25, 43). During the HSV-1 lytic cycle, vhs disables host protein synthesis and initiates mRNA degradation at the onset of infection and in later stages (22, 25, 31, 42). The vhs phosphoprotein is 489-amino-acids in length and targets mRNA for cleavage at non-sequence specific sites. Functional VP16 is necessary as a deactivator of vhs at the later stages of the cycle; virions are not assembled when VP16 that cannot bind to vhs (29, 33, 47). VP16 is also responsible for incorporating bound vhs into the tegument.

HSV-1 VP16 is approximately 490-residues in length and contains an acidic carboxy-terminal transcriptional activation domain. Deletion of this domain cripples the ability of VP16 to transactivate IE genes (20). Crystal structures characterizing the conserved core of VP16, have identified several surface residues that are important for interaction with DNA and the VIC complex (see Figure 10).

E. Purpose and Overview of Two Studies Concerning VP16

The two studies to be discussed are, “DNA recognition by the herpes simplex virus transactivator VP16: a novel DNA-binding structure” and “A single amino acid substitution in herpes simplex virus type 1 VP16 inhibits binding to the virion host shutoff protein and is incompatible with virus growth” (4, 20). These recent studies have identified VP16 DNA binding domain residues important for binding in the VIC complex and binding with vhs. Significant discoveries such as these not only expand knowledge about the herpes virus proteins and gene regulation, but also provide potential approaches to disrupting the lytic cycle of the virus (4, 20). Knez goes so far as to suggest that inhibitors of the VP16 complexes could be developed for use in antiviral therapeutics (20).

II. Materials and Methods

A. Cloning VP16

Site-specific VP16 mutations (for the second study to be discussed) were engineered by Knez et al. using Stratagene’s QuikChange® Site-Directed Mutagenesis Kit. The mutation of leucine 344 to alanine in VP16, the VP_(L344A) mutant, was found to be important to the study, rendering the cloning of this mutant equally important. The first step to constructing the VP_(L344A) mutant was site-directed mutagenesis of the *in vitro* transcription vector, pGEM5Zf(-)-VP404 (Promega). The pGEM5Zf(-)-VP404 “contains the *Nco*I/*Sac*II fragment” from “amino-terminal residues 1 to 404 of VP16” in its multiple cloning site (see Figure 11) (20).

QuikChange site-directed mutagenesis introduced the leucine 344 to alanine mutation into pGEM5Zf(-)-VP404 by using the oligonucleotide primer

5'-GTTGATTCGGGCGAAGCGGGACTCGTATTCCAG-3'

(the altered nucleotides are displayed and underlined, and the complimentary oligonucleotide is not shown). Site directed mutagenesis would have been performed on DNA isolated from *dam*⁺ *E. coli* strains, because these strains methylate their DNA. Purified pGEM5Zf(-)-VP404 was then added tubes containing *pfuTurbo*® DNA polymerase (a high fidelity DNA polymerase), the oligonucleotide primer displayed above, dNTP, buffer, and distilled-deionized water. The tubes would have run through about 12 thermal cycles in temperature cycler to activate 12 cycles DNA dissociation, annealing of primers, and DNA replication. During the last stage of each thermal cycle, the *pfuTurbo*® DNA polymerase, would have extended the two complimentary oligonucleotide primers using pGEM5Zf(-)-VP404 DNA as a template. This process would have produced a plasmid containing staggered nicks with the desired leucine 344 to alanine mutation. Upon completion of all 12 temperature cycles, *Dpn* 1, an endonuclease that targets methylated DNA, would have been used to digest parental DNA while leaving the mutated plasmids intact. Subsequently, XL-1 Blue supercompetent cells would have been transformed with nicked mutant and control plasmid DNA. The transformants repair the nicks in the plasmids and would have been selected using antibiotic and color screening (46).

Once the VP_(L344A) mutation was made, the pGEM5Zf(-)-VP404_(L344A) plasmid was digested with *Sal*I and *Sac*II once again to obtain a fragment of VP16 with the mutation. Knez's study uses the mammalian expression vector pEVRF65 in western blot analyses and virus complementation assays (40). While pEVRF65 vector expresses the entire wild-type VP16 gene, it has two *Sal*I sites; one at residue 5 and another at residue 411. Site-directed mutagenesis was employed to create a silent mutation at residue 411 and thus delete the *Sal*I site from pEVRF65. The sequences primers used in this reaction were 5'-CGCAGACTGTCTACGGCCCCCCC-3' and the complimentary oligonucleotide. The new *Sal*I deletion vector, pEVR65 Δ sal, was then

digested with *Sall* and *SacII*. The “*Sall/SacII* fragment was excised from pEVRF65 Δ sal and replaced with the corresponding *Sall/SacII* fragments” from the pGEM5Xf(-)-VP404_(L344A) mutant to create the pEVRF65_(L344A) clone (40).

Works Cited

1. **Ace, C. I., M. A. Dalrymple, F. H. Ramsey, V. O. Preston, and C. M. Preston.** 1988. Mutational analysis of the herpes simplex virus type I trans-inducing factor Vmw65. *J. Gen. Virol.* **69**:2595-2605.
2. **Ace, C. I., T. A. McKee, J. M. Ryan, J. Cameron, and C. M. Preston.** 1989. Construction and characterization of a herpes simplex virus type I mutant unable to transinduce immediate-early gene expression. *J. Virol.* **63**:2260-2269.
3. **Ausubel, F. M., R. Brent, R. E. Kingston, D. D. Moore, J. G. Seidman, J. A. Smith, and K. Struhl (ed.).** 1990. *Current protocols in molecular biology*. Wiley, New York, N. Y.
4. **Babb, R., C. C. Huang, D. J. Aufiero and W. Herr.** 2001. DNA recognition by the herpes simplex virus transactivator VP16: a novel DNA binding structure. *Mol. Cell. Biol.* **21**:4700-4712.
5. **Brar, D.** 2002. Cold Sores (HSV-1). Consumer Health Interactive. <http://www.principalhealthnews.com/topic/coldsores>. May 1, 2003.
6. **Brown, J. C.** Aug. 2002. Herpes Virus Research Laboratory; Background Information about Herpesviruses. <http://www.people.virginia.edu/~jcb2g/research/background.htm>. May 3, 2003.
7. **Chevray, P. M., and D. Nathanz.** 1992. Protein interaction cloning in yeast: Identification of mammalian proteins that react with the leucine zipper of Jun. *Proc. Natl. Acad. Sci. USA* **89**:5789-5793.
8. **Chou, P. Y., and G. D. Fasman.** 1978. Empirical prediction of protein conformation. *Annu. Rev. Biochem.* **547**: 251-276.
9. **Elgadi, M. M., C. E. Hayes, and J. R. Smiley.** 1999. The herpes simplex virus vhs protein induces endoribonucleolytic cleavage of target RNAs in cell extracts. *J. Virol.* **75**:7153-7164.
10. **Falcone, D., D. W. Andrews.** 1991. Both the 5' Untranslated region and the sequences surrounding the start site contribute to efficient initiation of translation in vitro. *Mol. Cell. Biol.* **11**:2656-2664.
11. **Feng, P., D. N. Everly, Jr., and G. S. Read.** 2001. mRNA decay during herpesvirus infections: interaction between a putative viral nuclease and a cellular translation factor. *J. Virol.* **75**:10272-10280.
12. **Fields, S., and O. Song.** 1989. A novel genetic system to detect protein-protein interactions. *Nature* **340**:245-247.
13. **Greaves, R., and P. O'Hare.** 1989. Separation of the requirements for protein-DNA complex assembly from those for functional activity in the herpes simplex virus regulatory protein Vmw65. *J. Virol.* **63**:1641-1650.
14. **Haigh, A., R. Greaves, and P. O'Hare.** 1990. Interference with the assembly of a virus-host transcription complex by peptide competition. *Nature (London)* **344**:257-259.
15. **Hay, J., and W. T. Ruyechan.** 1992. Regulation of herpes simplex virus type 1 gene expression. *Current Topics in Microbiology and Immunology.* **179**:1-11.
16. **Hayes, S., and P. O'Hare.** 1993. Mapping a major surface-exposed site in herpes simplex virus protein Vmw65 to a region of direct interaction in a transcription complex assembly. *J. virol.* **67**:852-862.
17. **Hughes, T., A. S. LaBoissiere, and P. O'Hare.** 1999. Analysis of functional domains of host cell factor involved in VP16 complex formation. *J. Biol. Chem.* **274**:16437-16443.

18. **International Herpes Management Forum.** 2003. Herpesviruses. <http://www.ihmf.org/general/HerpesVir.asp>. April 18, 2003.
19. **Karr, B. M., and G. S. Read.** 1999. The virion host shutoff function of herpes simplex virus degrades the 5' end of a target mRNA before the 3' end. *Virology* **264**:195-204
20. **Knez, J., P.T. Bilan, and J. P. Capone.** 2003. A single amino acid substitution in herpes simplex virus type 1 VP16 inhibits binding to the virion host shutoff protein and is incompatible with virus growth. *J. Virol.* **77**: 2892-2902.
21. **Kristie, T. M., and P. A. Sharp.** 1993. Purification of the cellular C1 factor required for the stable recognition of the Oct-1 homeodomain by the herpes simplex virus alpha-transinduction factor (VP16). *J. Biol. Chem.* **268**: 6525-6534.
22. **Kwong, A. D., and N. Frenkel.** 1987. Herpes simplex virus-infected cell contain a function(s) that destabilizes both host and viral mRNAs. *Proc. Natl. Acad. Sci. USA* **84**:1926-1930.
23. **LaBoissiere, S., T. Hughes, and P. O'Hare.** 1999. HCF-dependent nuclear import of VP16. *EMBO J.* **18**:480-489.
24. **Lai, J.-S., and W. Herr.** 1997. Interdigitated residues within a small region of VP16 interact with Oct-1, HCF and DNA. *Mol. Cell Biol.* **17**:3937-3947.
25. **Lam, Q., C. A. Simbert, K. E. Koop, C. Lavery, J. P. Capone, S. P. Weinheimer, and J. R. Smiley.** 1996. Herpes simplex virus VP16 rescues viral mRNA from destruction by the virion host shutoff function. *EMBO J.* **15**:2575-2581.
26. **Liu, Y., W. Gong, C. C. Haung, W. Herr, and X. Cheng.** 1999. Crystal structure of the conserved core of the herpes simplex virus transcriptional regulatory protein VP16. *Genes Dev.* **13**:1692-1703.
27. **Lu, P., F. E. Jones, H. A. Saffran, and J. R. Smiley.** 2001. Herpes simplex virus virion shutoff protein requires a mammalian factor for efficient in vitro endoribonuclease activity. *J. Virol.* **75**:1172-1185.
28. **Miyata, K. S., S. E. McCaw, H. V. Patel, R. A. Rachubinski, and J. P. Capone.** 1996. The orphan nuclear hormone receptor LXR α interacts with peroxisome proliferator-activated receptor and inhibits peroxisome proliferator signaling. *J. Biol. Chem.* **271**:9189-9192.
29. **Mossman, K. L., R. Sherburne, C. Lavery, J. Duncan, and J. R. Smiley.** 2001. Evidence that herpes simplex virus VP16 is required for viral egress down-stream of the initial envelopment event. *J. Virol.* **74**:6287-6299.
30. **O'Hare, P., and C. R. Goding.** 1988. Herpes simplex virus regulatory elements and the immunoglobulin octamer domain bind a common factor and are both targets for virion transactivation. *Cell* **52**:435-445.
31. **Osokar, A. A., and G. S. Read.** 1989. Control of mRNA stability by the virion host shutoff function of herpes simplex virus. *J. Virol.* **63**:1897-1906. **Pellett, P. E., J. L. C. McKnight, F. J. Jenkins, and B. Roizman.** 1985. Nucleotide sequence and predicted amino acid sequence of a protein encoded in a small herpes simplex virus DNA fragment capable of *trans*-inducing α genes. *Proc. Natl. Acad. Sci. USA.* **82**:8570-5874.
33. **Poon, A. P., and B. Roizman.** 1995. The phenotype in vitro and in infected cells of herpes simplex virus 1 alpha *trans*-inducing factor (VP16) carrying temperature sensitive mutations introduced by substitution of cysteines. *J. Virol.* **69**: 7658-7667. **Popova, B., P. Bilan, P. Xiao, M. Faught, and J.P. Capone.** 1995. Transcriptional activation by DNA-binding derivatives of HSV1 VP16 that lack their carboxyl-terminal acidic activation domain. *Virology* **109**:19-28.
35. **Preston, C. M., M. C. Frame, and M. E. Campbell.** 1988. A complex formed between cell components and an HSV structural polypeptide binds to a viral immediate early gene regulatory DNA sequence. *Cell* **52**:425-434.
36. **Roizman, Bernard.** 2001. Herpesvirus Properties. <http://www.stdgen.lanl.gov/stdgen/bacteria/hhv1/herpes.html#intro>. April 18, 2003.

37. **Roizman, B., and D. M. Knipe.** 2001. Herpes simplex viruses and their replication. P. 2399-2459. In D. M. Knipe and P. M. Howley (ed.). *Fields virology*. Lippincott Williams and Wilkins, Philadelphia, Pa.
38. **Sadowski, I., J. Ma, S. Triezenberg, and M. Ptashne.** 1988. Gal4-VP16 is an unusually potent transcriptional activator. *Nature (London)* **344**:563-564.
39. **Schmelter, J., J. Knez, J. R. Smiley, and J. P. Capone.** 1996. Identification and characterization of a small modular domain in the herpes simplex virus host shutoff protein sufficient for interaction with VP16. *J. Virol.* **70**:2124-2131.
40. **Shaw, P., J. Knez, and J. P. Capone.** 1995. Amino acid substitutions in the herpes simplex virus transactivator VP16 uncouple direct protein-protein interaction and DNA binding from complex assembly and transactivation. *J. Biol. Chem.* **270**:29030-29037.
41. **Simmen, K. A., A. Newell, M. Robinson, J. S. Mills, G. Canning, R. Handa, K. Parkes, N. Borkakoti, and R. Jupp.** 1997. Protein interactions in the herpes simplex virus type 1 VP16-induced complex: VP16 peptide inhibition and mutational analysis of host cell factor requirements. *J. Virol.* **71**:3886-3894.
42. **Simbert, C. A., D. C. Johnson, and J. R. Smiley.** 1992. Identification and characterization of the virion-induced shutoff product of herpes simplex virus gene UL41. *J. Gen. Virol.* **73**:477-470.
43. **Simbert, C. A., B. Popova, P. Xiao, J. P. Capone, and J. R. Smiley.** 1994. Herpes simplex virus VP16 forms a complex with the virion host shutoff protein vhs. *J. Virol.* **68**:2339-2347.
44. **Smiley, J. R., and J. Duncan.** 1997. Truncation of the C-terminal acidic transcriptional activation domain of herpes simplex virus VP16 produces a phenotype similar to that of the in1814 linker insertion mutation. *J. Virol.* **71**:6191-6193.
45. **Stannard, L. M.** 1995. Herpesvirus. <http://web.uct.ac.za/depts/mmi/stannard/herpes.html>. April 13, 2003.
46. **Stratagene.** 2003. QuikChange® Site-Directed Mutagenesis Kit; Instruction Manual. Revision #043008k.
47. **Wagner, E. K.** Oct. 2002. The Homepage of Dr. Edward K. Wagner. <http://darwin.bio.uci.edu/%7Eefaculty/wagner/index.html>. April 18, 2003.
48. **Weinheimer, S. P., B. A. Boyd, S. K. Durham, J. L. Resnick, and D. R. O'Boyle II.** 1992. Detection of the VP16 open reading frame of herpes simplex virus type I. *J. Virol.* **66**:258-269.
49. **Werstuck, G., P. Bilan, and J. P. Capone.** 1990. Enhanced infectivity of herpes simplex virus type 1 viral DNA in a cell line expressing *trans*-inducing factor Vmw65. *J. Virol.* **64**:984-991.
50. **Werstuck, G., and J. P. Capone.** 1989. Identification of a domain of the herpes simplex virus *trans*-activator Vmw65 required for Protein-DNA Complex formation through the use of protein A fusion proteins. *J. Virol.* **63**:5509-5513.
51. **Werstuck, G., and J. P. Capone.** 1989. Mutational analysis of the herpes simplex virus immediate-early *trans*-inducing factor Vmw65. *Gene* **75**:213-224.
52. **Wilson, A. C., K. LaMarco, M. G. Peterson, and W. Herr.** 1993. The VP16 accessory protein HCF is a family of polypeptides processed from a large precursor protein. *Cell* **74**:115-125.
53. **Wu, T. J., G. Monokian, D. F. Mark, and C. R. Wobbe.** 1994. Transcriptional activation by herpes simplex virus type I VP16 in vitro and its inhibition by oligopeptides. *Mol. Cell. Biol.* **14**:3484-3493.
54. **Xiao, P., and J. P. Capone.** 1990. A cellular factor binds to the herpes simplex virus type I transactivator Vmw65 and is required for Vmw65-dependent protein-DNA complex assembly with Oct-1. *Mol. Cell. Biol.* **10**:4974-4977.

Impact of Water Lilies (*Nymphaea tuberosa*) on Predator-Avoidance Behavior of *Daphnia magna*

Lisa M. Harsch and Romi L. Burks

Abstract

Daphnia magna, a common species of freshwater large-bodied zooplankton, undergo diel horizontal migration (DHM) into littoral zones in shallow lakes as a means of predator avoidance. We wanted to determine how different refuge properties of floating-leaved macrophytes, e.g the white water lily, *Nymphaea tuberosa*, influenced the survival of *Daphnia*. For example, stem density of *Nymphaea* might provide complexity while the floating leaves, or pads, could lower light penetration. This experiment tested whether the submerged vegetation, floating canopy, or both proved necessary to attract *Daphnia* and increase their survival against predators during both day and night. We used zooplanktivorous fish and larval odonates, dragonflies, as predators to determine the refuge effects of the macrophytes. Surprisingly, we found no difference in abundance during day and night. However, according to *Daphnia* abundance results pooled among all samples taken from different treatments, the presence of submerged structure significantly increased *Daphnia* survival. Overall, our results showed that, in contrast to the control groups containing no plants, floating-leaved macrophytes did serve as a reasonable refuge against predation. However, mortality rates remained high within them and any refuge provided depended on the submerged complex structure.

Introduction

Submerged macrophytes play an important role in the ecosystem of shallow freshwater lakes. They are the main impetus behind maintaining a state of clear water versus turbid (Moss, 1998) as well as for providing a refuge to phytoplankton-grazing

zooplankton (Carpenter and Lodge, 1986; Lauridsen *et al.*, 1996; Burks *et al.*, 2002).

Turbid water occurs when a lake experiences eutrophication in which there is an excess of nutrient loading (phosphorus and nitrogen) which causes an increase in phytoplankton growth (Lauridsen *et al.*, 1996; Moss, 1998). Macrophytes compete with phytoplankton, commonly called algae, for nutrients (Cattaneo *et al.*, 1998; Moss *et al.*, 1998) and also cause significant changes to abiotic of the water including light, temperature and dissolved oxygen concentration (Frodge *et al.*, 1990; Diehl and Kornijow, 1998).

Zooplankton and other microinvertebrates graze on the phytoplankton and epiphyton which also attributes to the clear water state (Moss, 1998). Macrophytes function in providing a refuge for zooplankton from predation by certain zooplanktivorous fishes (Burks *et al.*, 2001a). Such fishes, generally juvenile piscivores or small planktivores, also use macrophytes as refuge from adult piscivores (Chick and McIvor, 1994; Jeppesen *et al.* 1997; Moss *et al.*, 1998). In addition, macrophytes serve as habitats for larval odonates and other benthic predators (Burks *et al.*, 2001b). The amount of plant density is thought to be negatively related to zooplankton mortality (Schriver *et al.*, 1995; Jeppesen *et al.*, 1997).

Daphnia, a large-bodied zooplankter, is a commonly-found grazer in shallow lake systems. These microcrustaceans, known as water fleas, are commonly studied due to their wide distribution as well as their ability to survive well in culture. Although large compared to other pelagic zooplankton, *Daphnia* can be considered an intermediate size in comparison with all zooplankton. Thus, theoretically, they represent a median for the study of zooplankton, especially in their effects on the ecology of shallow waters (De Bernardi and Peters, 1987).

When coming into contact with pelagic fishes, recent studies have indicated that, *Daphnia* commonly undergo diel horizontal migration (DHM) into littoral zones as a predator-avoidance strategy (White, 1998; Blindow *et al.*, 2000; Burks *et al.*, 2001a). This is a behavior recognized in shallow water as opposed to deep water where studies demonstrate that *Daphnia* undergo diel vertical migration (DVM) as a form of predator avoidance (Stich and Lampert 1984). In areas where DVM takes place, *Daphnia* avoid littoral areas and maintain themselves as an open water genus (Burks *et al.*, 2001a). Considering the general avoidance of plants, it is important to determine the effectiveness and mechanism behind the use of macrophytes for protection. This information has not been studied well.

For floating-leaved macrophytes, the predator avoidance action could be signaled by the floating portion of the plant which creates a canopy over the water that blocks light from entering (Frodge *et al.* 1990; Olson, 1995). Alternatively, the movement could be caused by the structural complexity created within the submerged stems of the plants. Identification of the actual stems or the general chemical cues that they give off (Ostrofsky and Zettler, 1986; Dorn *et al.*, 2001) rather than the effects perceived from light may prompt the *Daphnia* (Marklund *et al.* 2001). The full effect of both stems and floating canopy together may be required to initiate this diel horizontal movement among *Daphnia*.

In our study, we wished to identify the key factors behind *Daphnia* predator-avoidance movement into floating-leaved macrophytes by determining the daphnid response to environments with only floating canopy, only submerged macrophyte stems, or both canopy and stems. These treatments acted to separate the specific refuge

The stem densities of all *Nymphaea* were statistically the same before alteration into treatments (Fig. 2; 1-way ANOVA $p < 0.05$). Although we collected more *Daphnia* at night, no significant difference existed in the abundance of *Daphnia* at night versus during the day (Fig. 3; 3-way ANOVA $F_{1,128} = 0.886$, $p = 0.348$). In addition, we did not find a statistical difference between the abundance of *Daphnia* found at the upper surface of the tubs versus the bottom (Fig. 4; 3-way ANOVA $F_{1,128} = 1.362$, $p = 0.245$). For these reasons, we pooled all daphnid abundance data to determine the overall impact of the treatments.

We found that *Daphnia* abundance did significantly differ between treatments (Fig. 5; 1-way ANOVA $p = 0.014$). The “stems only” treatment did not differ from the “canopy only” treatment (Tukey’s MCT $p = 0.161$) but it did differ from the treatments containing “both stems and canopy” as well as the control groups (Tukey’s MCT $p = 0.020$, 0.023 , respectively). The other three treatments did not show any significant differences between them (Tukey’s MCT all p -values > 0.05). The presence of predators played an extreme role on the mortality of the daphnids in every treatment expressed in the low capture among each treatment ($n \leq 24$).

A considerable number of other invertebrates that were not originally placed in the experimental tubs occurred in the samples. The abundance of *Choaborus* dominated in the “stems only” treatments more than any of the others (Fig. 6a; Tukey’s MCT $p < 0.05$). We found the abundance of mosquito larva to be significantly greater among the “canopy only” treatments than the other treatments (Fig. 6b; Tukey’s MCT $p < 0.05$). An excessive number of Copepods occurred almost exclusively in the control groups (Fig. 6c Tukey’s MCT $p = 0.027$). The number of *Eurycercus* found in each treatment did

the center, and one from the center (Figure 1). Different sampling positions insured that all distributions of *Daphnia* are considered. After sampling, we filtered the contents through a 50- μ m mesh filter and then preserved the contents in vials with Lugol's solution for later enumeration. We examined the samples under a dissecting microscope to determine zooplankton abundance. We took recordings of the number of *Daphnia*, mosquito larva, *Chaoborus*, copepods, and *Eurycercus* present in each sample. No other invertebrates occurred in the samples.

We used the number of *Daphnia* present as the dependent variable in a 3-way analysis of variance (ANOVA) to determine differences among time (day vs. night) sampling position (top vs. bottom) and treatment (stems, no stems, or both). Pooling non-significant factors, we used a 1-way ANOVA to determine differences between overall treatments followed by a *post hoc*, Tukey's multiple comparison test to compare differences between treatments. We used these tests to determine whether the presence of structure, canopy, or both produced a significant impact of the mortality rate of *Daphnia* among natural predation.

Abiotic conditions

We monitored abiotic conditions in order to exclude alternative explanations for the differences between treatments. Temperature and dissolved oxygen (DO) readings of the surface, middle and bottom of each experimental tub occurred routinely. We took measurements of water clarity using a Secchi disk.

Results

Outdoor Laboratory Study

the bottom to determine *Daphnia* situational preference within the stratification of the experimental environment. The third treatment (both stems and canopy) leaves the water lilies completely intact. The final three tubs remained as controls, containing no plants but the same amount of soil and predators.

Once the plants developed, the actual predation experiment began. We enumerated the stem density of each tank to maintain uniformity between tanks. We cultured *Daphnia* within the lab until time for their placement in the experimental tubs. Each tub received an initial concentration of approximately 900 daphnids. Common goldfish, *Carassius auratus*, acted as the representative zooplanktivorous fish, due to their availability and the mortality rate of other species. We also gathered larval odonates of varying sizes from a local pond. Each tub contained one goldfish, one large, larval odonate, *Somatochlora ozarkensis*, between 0.2g-0.4g and a few smaller larval odonates with a combined mass of approximately 0.4g to create natural predation for *Daphnia*.

Zooplankton Sampling

The experiment lasted approximately two weeks and included several samplings. We added the initial concentration of daphnids to each tub at the beginning of the first week. We collected 3 sets of paired day/night samples (Day 3/5, 7, and 11/12). We sampled the tubs using a tube sampler (height = 44-cm). Measured on the tube, a 14-cm sample holding approximately 450-mL of water represented "top" samples and a 29-cm sample holding approximately 1.06 L of water taken from the entire depth of the tub constituted the whole sample. In each tub, we took three samples from the top for a combined top sample and three samples from the bottom for a combined bottom sample. One sample occurred near the outside edge, one from the middle between the outside and

mechanisms. We also examined diel effects in relation to nighttime versus daytime when fish are considered to be more active as visual predators (Lauridsen *et al.*, 1996; White, 1998). To assess the impact of multiple predators, as would be present in nature, we also included larval dragonflies in our study which are benthic predators known to feed on *Daphnia* when present (Burks *et al.*, 2001b). Together, these predators provided an effective environment for investigating the mechanism of predator-defense among macrophytes.

Methods

Outdoor Laboratory Study

The research took place in an outdoor courtyard at Rhodes College in Memphis, TN in late summer. We used 12, large 54-gallon black tubs for the experiments. The water lilies, *Nymphaea tuberosa*, occurred in 9 of the tubs, planted in May, allowing 3 for controls. We divided the original *Nymphaea* tubers into 3 groups of small, medium and large. Each of the tanks received approximately 40 small tubers, each with a weight below 5.5g, 45 medium tubers ranging from 5.5g- 13g and 3 large tubers with weight greater than 13g. We allowed 3 months for growth. The experiment took place in an outdoor uncovered courtyard in order to create a natural environment subject to all naturally occurring weather and insects.

Before adding any animals to the experiment, we assigned the tubs to four different treatments. In the first treatment (stems only), we removed all of the floating vegetation from the plants leaving only the submerged stems. In the second treatment (canopy only), floating tops remained but we cut the submerged stem from the water surface to approximately two inches from the soil bottom. We left minimal vegetation at

not statistically differ but it appeared to be much greater among the ‘‘canopy only’’ and control treatments, those treatments containing no submerged vegetation (Fig. 6d).

Abiotic conditions

The overall temperature did not differ significantly among tubs with the exception of the surface temperature being slightly lower in the tanks containing the full plant, stems and canopy (Table 2; 3-way ANOVA_{1,8} F = (top) 6.923, (mid) 5.677, (bot) 21.790 all *p*-values < 0.05). We found dissolved oxygen (%) to be significantly different between treatments as well as differing between surface, middle, and bottom (Fig. 7; Tukey’s MCT all *p*-values < 0.05). The ‘‘stems only’’ treatment had the highest percent followed by the control group. The two groups which contained a floating-leaf canopy (‘‘canopy only’’ and ‘‘both stems and canopy’’) were found to have much lower percentage than the other two. Water clarity tested with a Secchi disk proved to be fairly similar between the treatment groups in contrast to that of the control groups which experienced an exceptionally high level of clarity.

Table 1. Mean temperature, dissolved oxygen, and water clarity through Secchi disk measurement (\pm 1 standard deviation).

Treatment	Mean Temp. °C		Dissolved Oxygen		Secchi Disk in cm
‘‘Stems Only’’	Surface	32.37 \pm 0.47	Surface	17.17 \pm 2.02	11.67 \pm 2.89
	Middle	31.3 \pm 1.15	Middle	10.17 \pm 6.07	
	Bottom	30.53 \pm 0.45	Bottom	5.75 \pm 2.22	
‘‘Canopy Only’’	Surface	32.53 \pm 0.31	Surface	8.39 \pm 3.19	10.0 \pm 2.0

	Middle	31.60 ± 0.50	Middle	4.48 ± 2.16	
	Bottom	29.37 ± 0.59	Bottom	0.64 ± 0.48	
"Both"	Surface	31.10 ± 0.20	Surface	6.11 ± 4.84	16.67 ± 4.73
	Middle	30.33 ± 0.57	Middle	2.13 ± 1.20	
	Bottom	29.77 ± 0.21	Bottom	1.86 ± 1.79	
Control	Surface	32.23 ± 0.40	Surface	12.35 ± 1.77	29.0 ± 3.61
	Middle	31.40 ± 0.72	Middle	12.18 ± 2.02	
	Bottom	29.47 ± 1.42	Bottom	9.66 ± 0.90	

Figure 1.

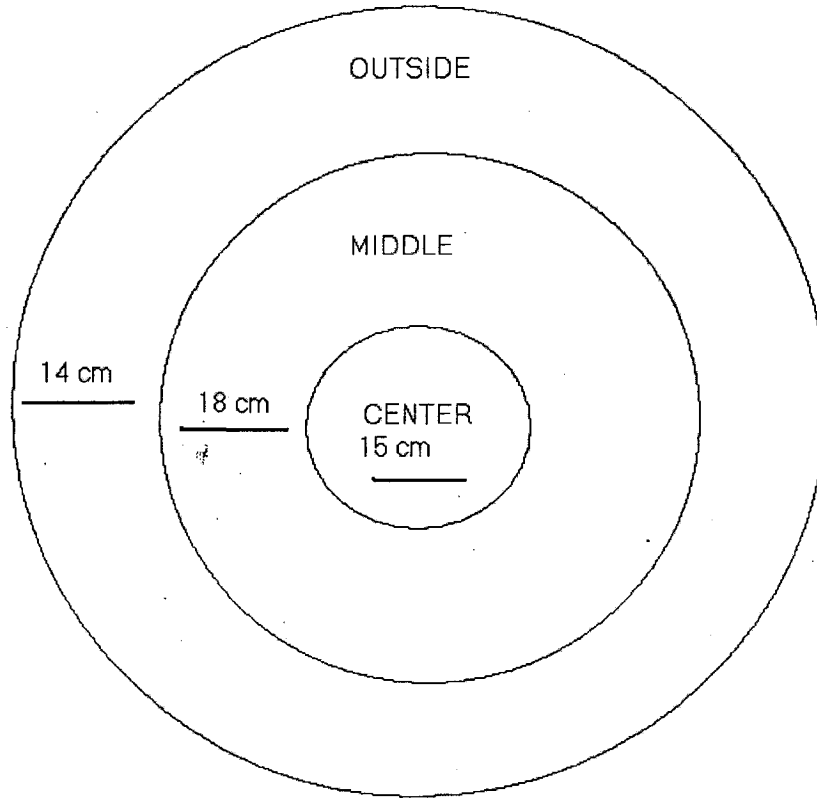


Figure 1. A surface view of the tubs which indicates the three positions in which we took samples.

Figure 2.

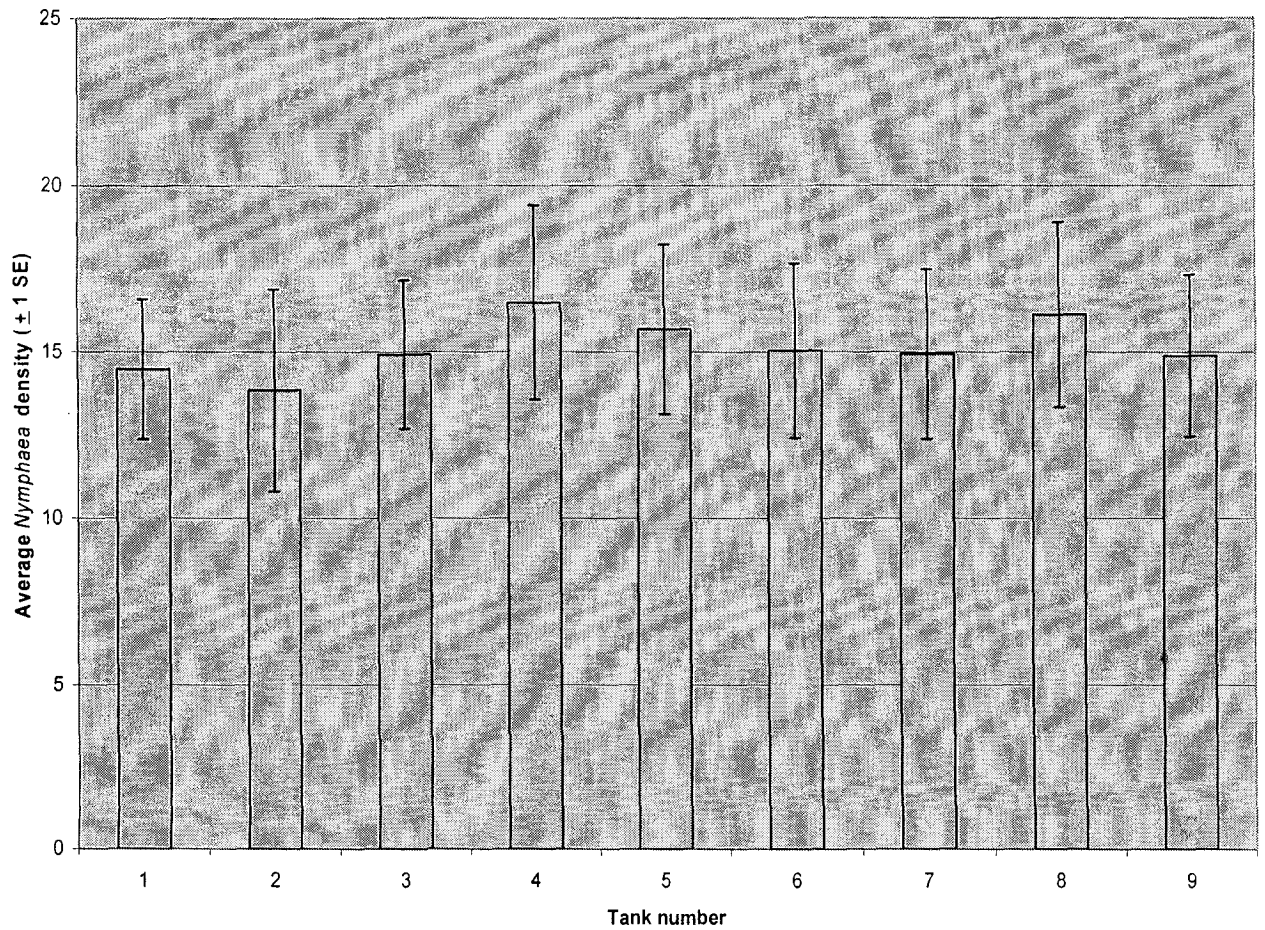


Figure 2. The average stem densities found among *Nymphaea tuberosa* in the tubs before transformations into different treatments for use in the experiment

Figure 3.

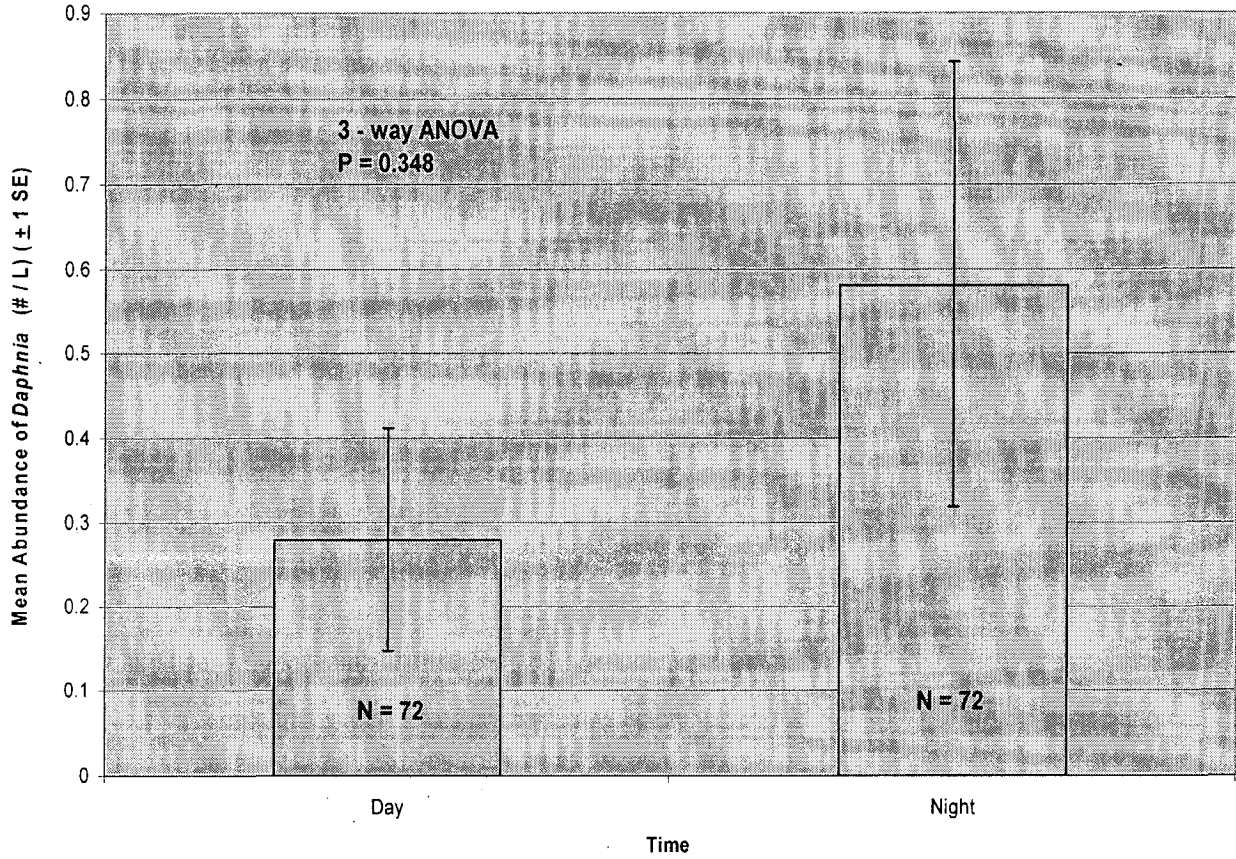


Figure 3. A display of the mean abundance of *Daphnia* recovered during the night versus those recovered during the day. Absence of any asterisk indicates the lack of statistical difference.

Figure 4

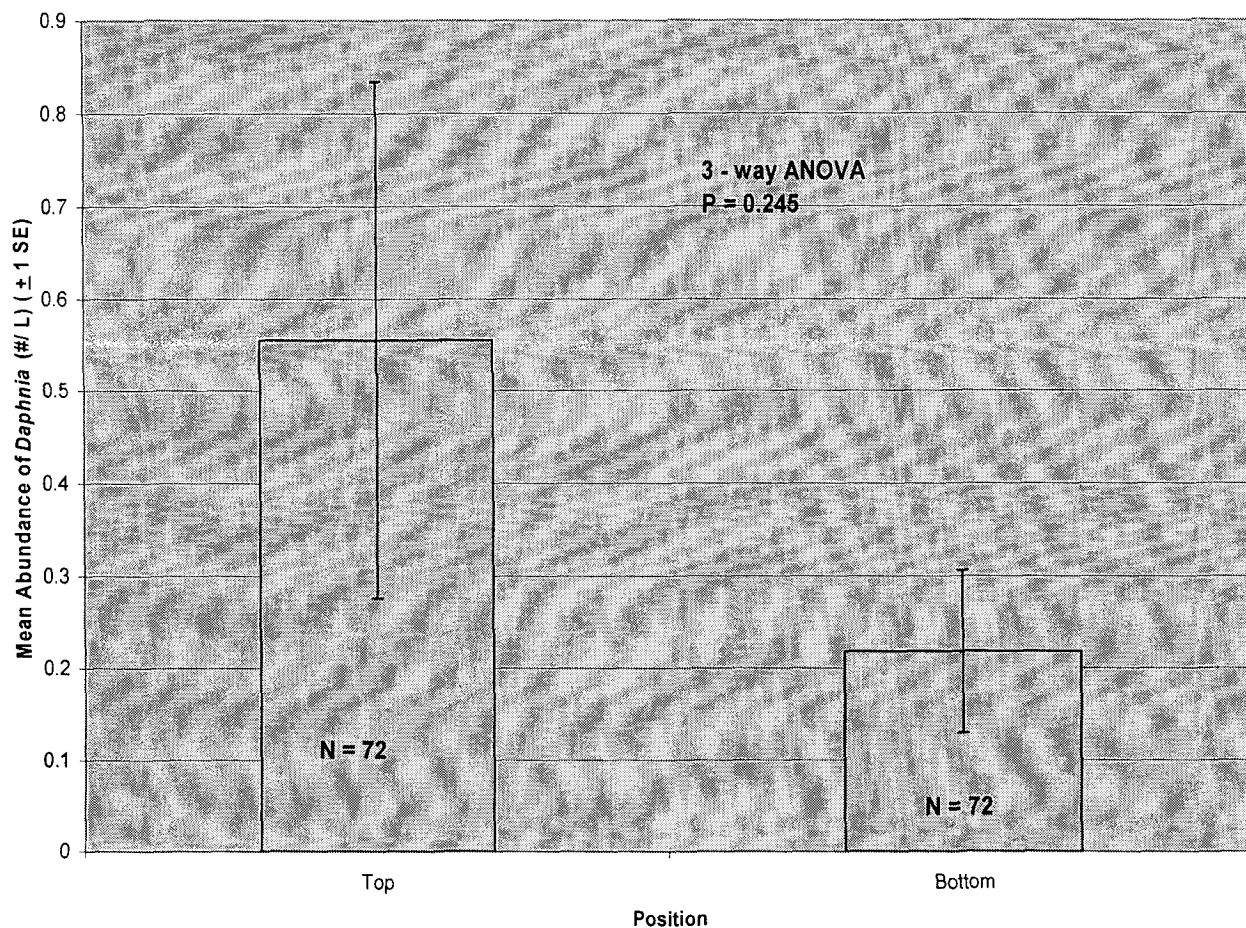


Figure 4. The mean *Daphnia* abundance we collected from samples taken from the top versus those taken from the whole length of the tub including bottom.

Figure 5.

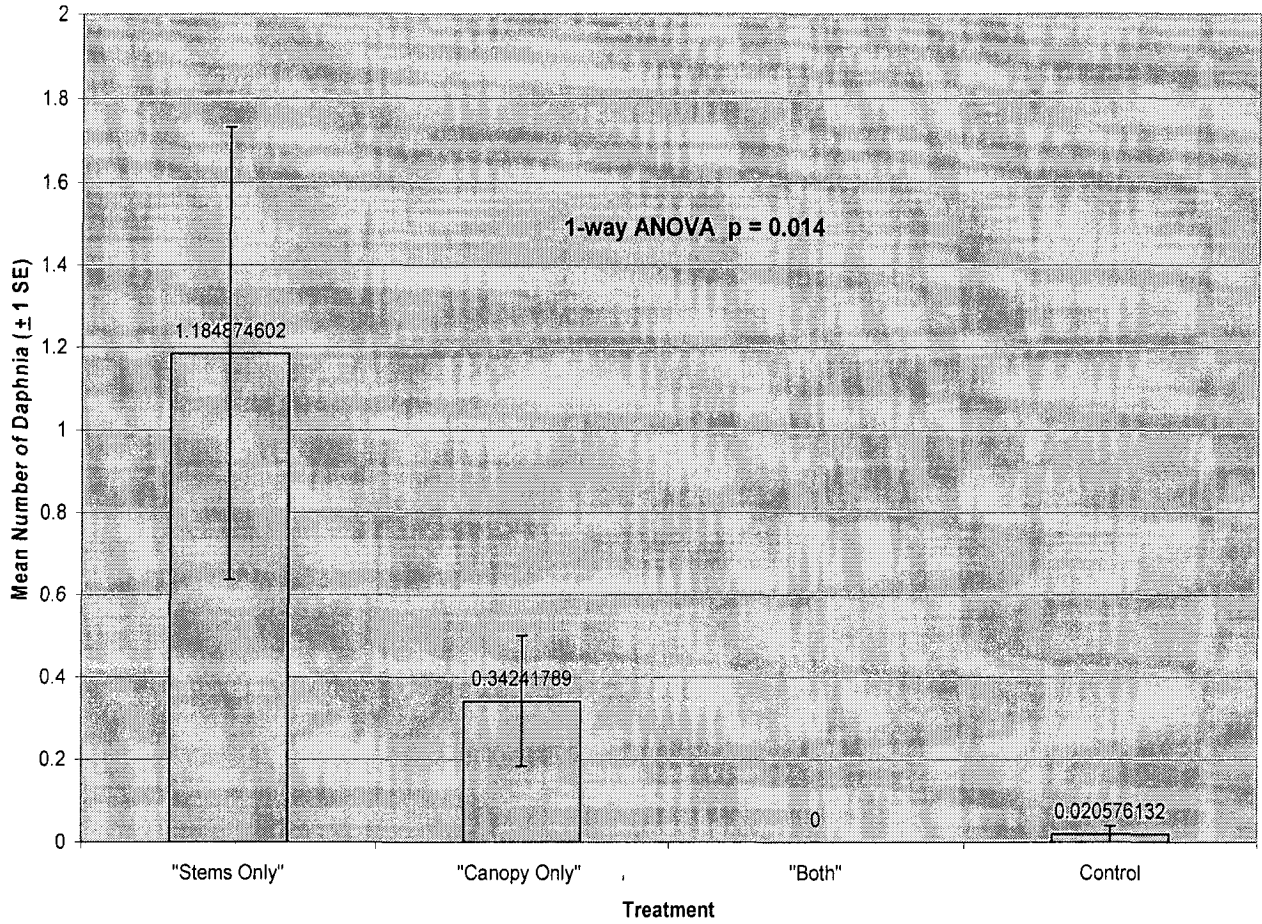


Figure 5. A significantly greater abundance of *Daphnia* occurring in the “stems only” groups as compared with the lower abundance occurring within the other treatments.

Figure 6a.

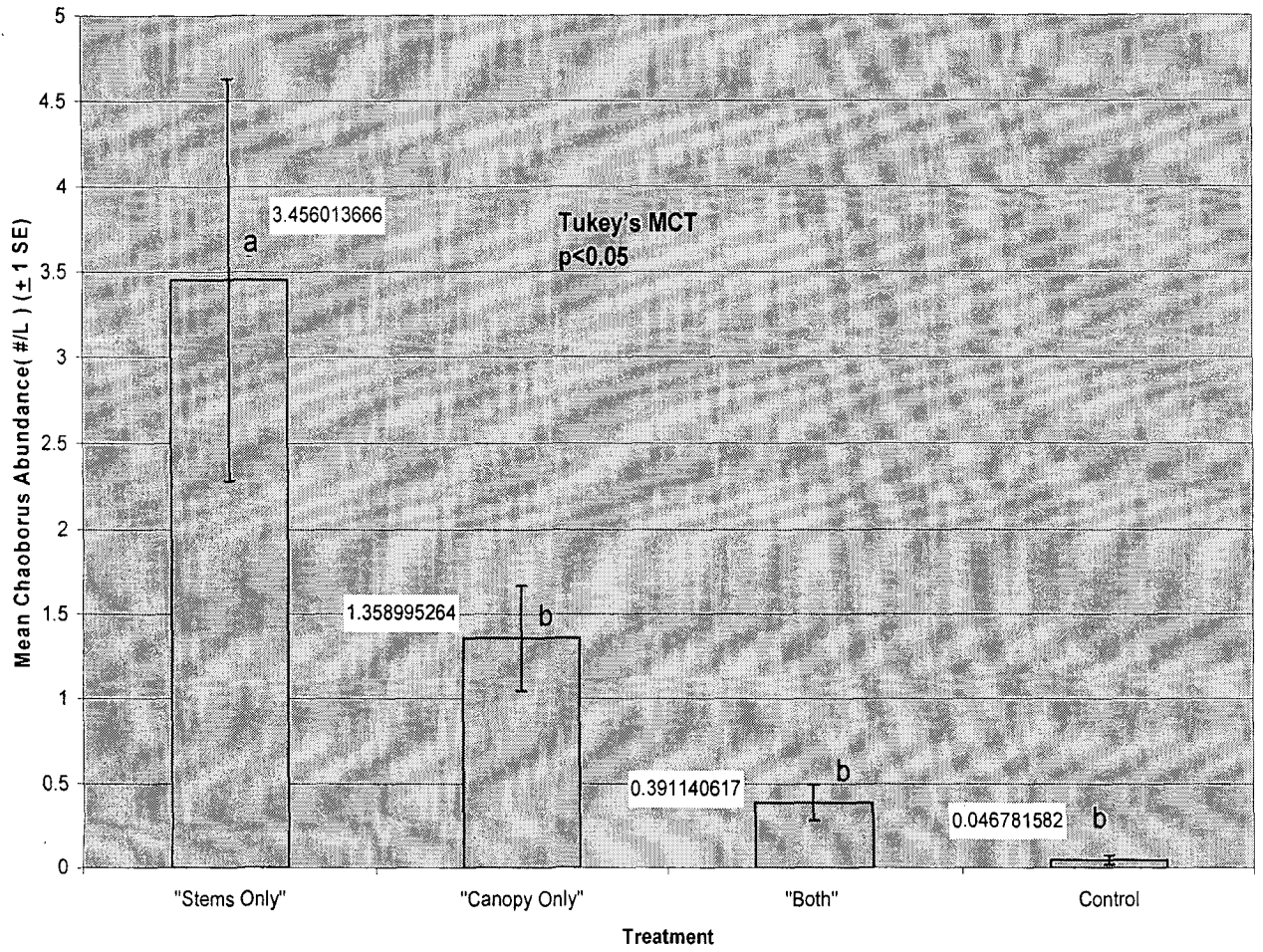


Figure 6a. The abundance of *Chaoborus* occurring within the different tubs.

Figure 6b.

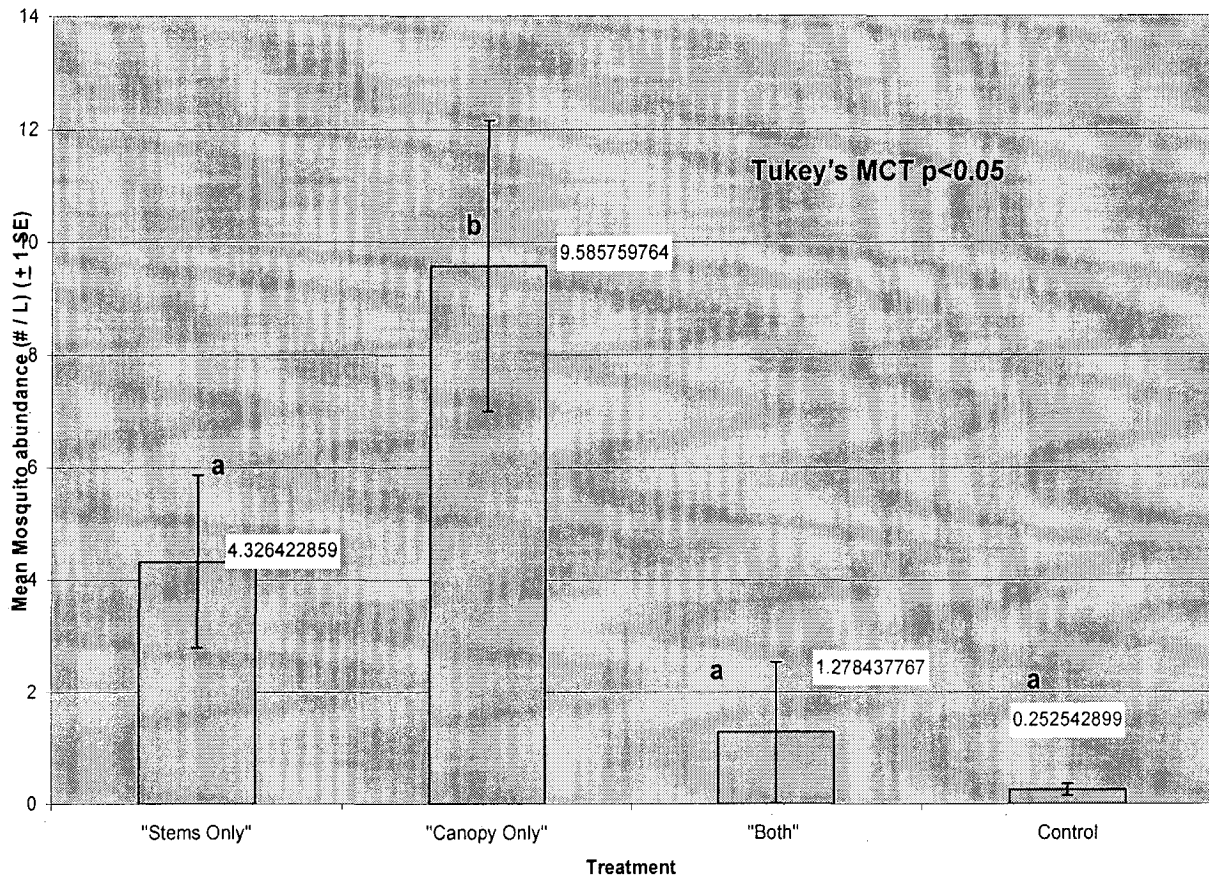


Figure 6b. The amount of mosquito larva occurring in the tubs compared with the treatment in which it was persisting.

Figure 6c.

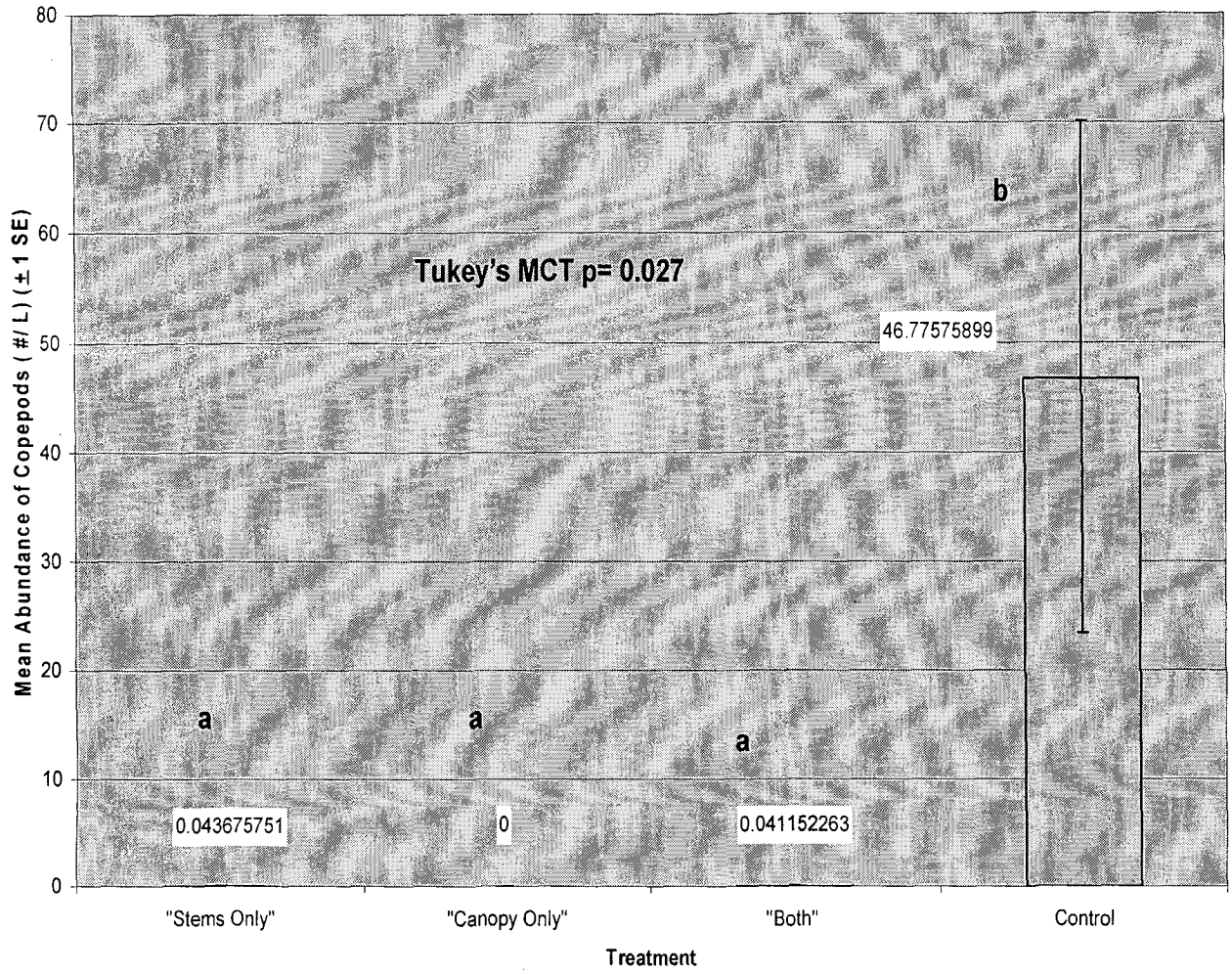


Figure 6c. The mean abundance of copepods occurring within the treatments.

Figure 6d.

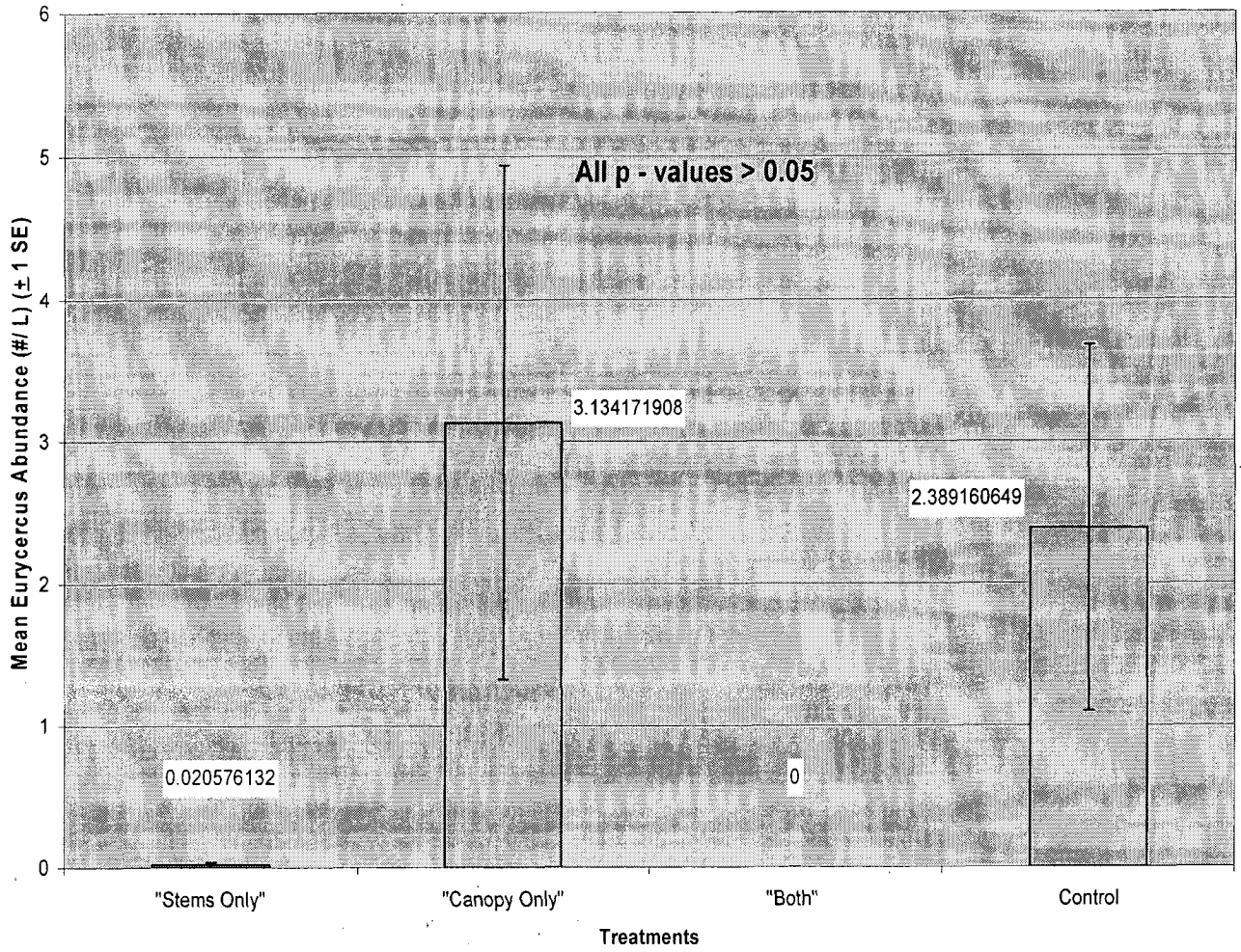


Figure 6d. The mean *Eurycercus* abundance occurring within the different treatments.

Figure 7.

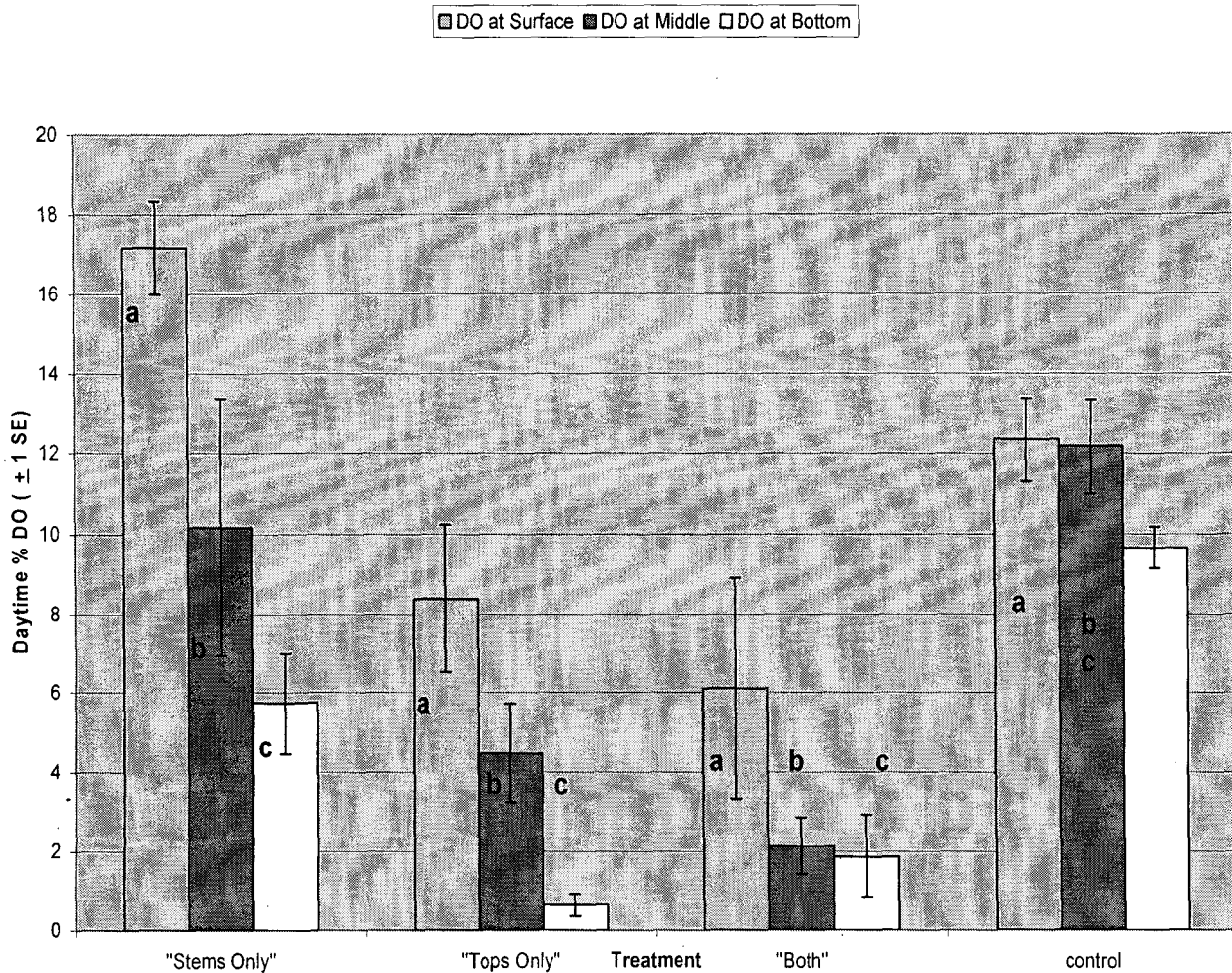


Figure 7. The mean dissolved oxygen concentration found in the surface, middle, and bottom layers of the different tubs compared with treatment.

Figure 8.

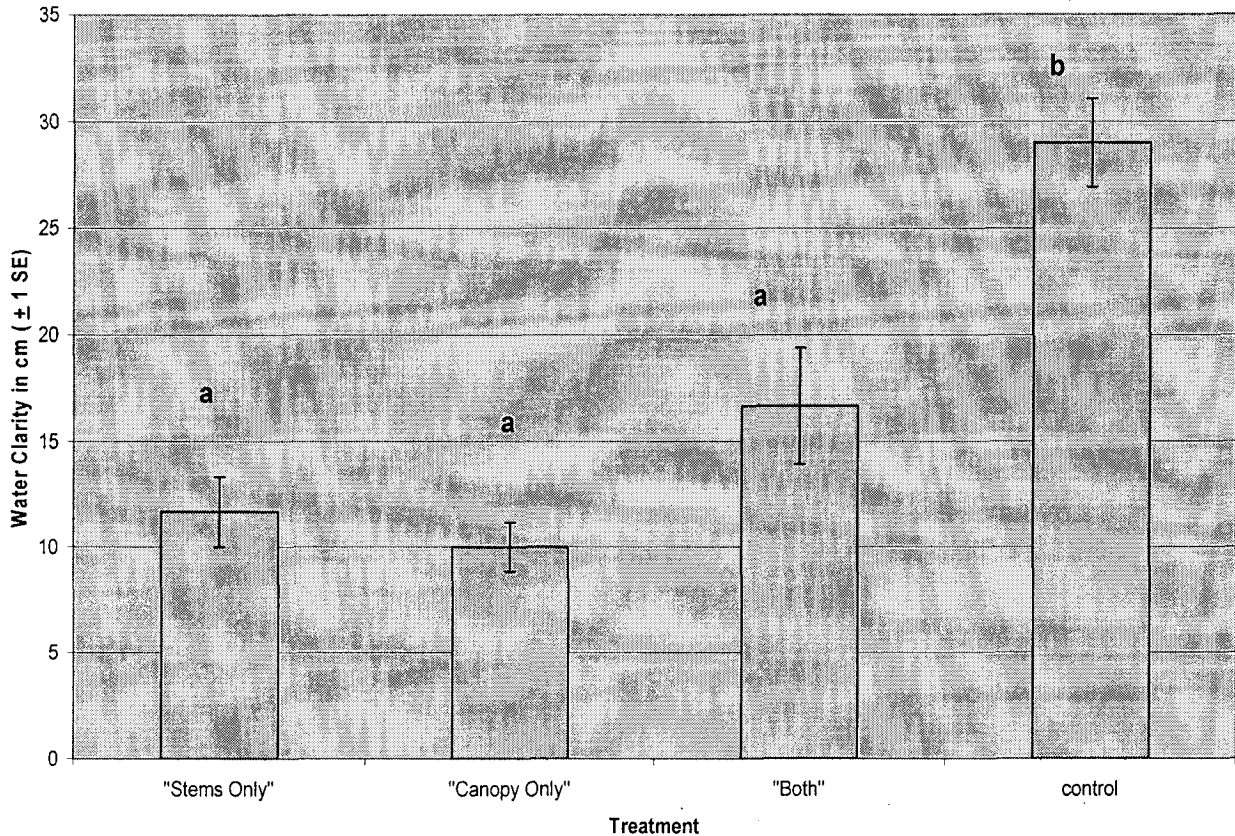


Figure 8. Results of the amount of water clarity found with in each tub in comparison with its treatment.

Discussion

High *Daphnia* mortality occurred throughout all divisions of the experiment. The multiple predators consumed nearly all specimens. The "stems only" experimental tubs showed the most significant potential for predator avoidance by the number of *Daphnia* recovered. Our results are comparable to other experiments which indicate that an increase in density and complexity of the macrophytes is positively correlated with a decrease in predation (Winfield, 1986; Jeppesen *et al.*, 1997; Burks *et al.*, 2001). This decrease may occur because prey fish prefer sparse vegetation, thus keeping

planktivorous fish within minimal densities (Jeppesen *et al.*, 1997; Murklund *et al.*, 2001). The difference, however, is that in this experiment the “both stems and canopy” tubs did not display a significant role as an anti-predator refuge. Thus, it remains a bit perplexing as to why the addition of the canopy negated the refuge effect instead of supplementing it.

The “tops only” tubs, or canopy alone, did not appear to serve as a refuge. These results lead to the indication that the canopy creates its own effect. According to Frodge *et al.* (1990), development of dense macrophyte canopies contributes to a partitioning of the littoral water column into areas with distinct physical and chemical characteristics. One of these characteristics is change in the lighting. This lack of lighting would presumably be linked to inefficiencies among visual predators. However, several studies contradict this notion (Blois-Heulin *et al.*, 1990; Moss *et al.*, 1998; Burks *et al.*, 2001). According to our water clarity results using the Secchi disk, the depth of light penetration within the different treatments was basically the same, thus indicating some other reason for our results.

If low light cannot explain our results, dissolved oxygen (DO) could have produced an impact. In our experiment, significant differences in DO existed between those experimental tubs which contained a form of canopy (“canopy only” and “Both”) and those which contained no form of canopy (“stems only” and control). The DO in the canopy tubs was lower overall than that found in the non-canopy tubs. This is consistent with other experiments that indicate that the canopy of floating leaves reflects a marked change in DO concentration (Carpenter and Lodge, 1986; Frodge *et al.*, 1990). Further experimentation is needed to elaborate on the idea of DO being the reasoning for

Daphnia movement into littoral zones. Other abiotic conditions did not seem to differ very greatly between treatments, thus indicating their lack of significance in the defense mechanism.

Other factors may also be associated with the canopy. Several studies investigate the idea of chemical cues from plants (Olson *et al.*, 1995; Burks *et al.*, 2001; Burks and Lodge, 2002). Many herbivores feed on aquatic plants. In defense of this herbivory, many plants produce toxins which deter the predator either immediately or over time (Cronin, 1997; Dorn *et al.*, 2001). These chemical toxins may be released into the water, thus signaling the dispersal of any microinvertebrates especially *Daphnia* (Lauridsen and Lodge, 1996). This mirrors the influence of chemical cues thought to be released from other predators (Kvam and Kleiven, 1995; Bronmark and Hansson, 2000). The chemicals are supposedly found within the leaves of the macrophytes (Ostrofsky and Zettler, 1986), which could indicate why the canopy of the *Nymphaea* produced negative refuge effects.

A significantly higher presence of *Chaoborus* within the “stems only” treatments versus the other treatments serves as an additional factor that suggests the stems to provide adequate predator refuge. *Chaoborus* feed on juvenile daphnids, thus providing an additional predator to the *Daphnia* population within the tubs. According to Kvam and Kleiven (1995), *Daphnia* species respond to chemical signals from *Chaoborus* and change their migration patterns. *Chaoborus* eat significantly more daphnids in the light thus illustrating their dependence on visual prey detection (Kvam and Kleiven, 1995). The submerged density of the plants may produce a visual deterrence for *Chaoborus*. The fact that they are more heavily present in the “stems only” tubs indicates that they

may too be influenced by abiotic conditions. Their lack of presence in the control groups demonstrates the further effects of the stems in providing protection from predators for them as well. In lakes where *Chaoborus* and *Daphnia* coexist, more studies are necessary to better understand their relationship with macrophytes.

Results from this experiment contradict the idea that a difference exists in *Daphnia* location between day versus night. *Daphnia* are considered to be an open-water genus (Moss *et al.*, 1998) that undergoes diel horizontal migration (DHM) in to the littoral zone during the day for protection from zooplanktivorous fish (Jeppesen *et al.*, 1997; White, 1998; Burks *et al.*, 2001). Our results did not find any significant difference between the abundance of *Daphnia* among all treatments during the day versus their abundance during the night. This, however, is complementary to other experiments which have experienced the same results (Lauridsen *et al.*, 1996; Murklund *et al.*, 2001).

Macrophytes provide a refuge for shallow water grazing *Daphnia* from predators. The mechanism of this refuge within floating-leaved macrophytes centers on the complexity of the stems alone with the presence of the canopy leaves having negative effects. Further research among the differences between floating-leaved and submerged macrophytes is necessary to determine the relationship between the stems and the refuge. Abiotic conditions appear to be provide the probable reasons; however, more detailed studies of these aspects are needed.

References

- Blindow, I., Hargeby, A., Wagner, B. M. A., and Andersson, G. 2000. How important is the crustacean plankton for the maintenance of water clarity in shallow lakes with abundant submerged vegetation? *Freshwater Biology* 44: 185-197.
- Blois-Heulin, C., Crowley, P. H., Arrington, M., and Johnson, D. M. 1990. Direct and indirect effects of predators on the dominant invertebrates of two freshwater littoral communities. *Oecologia* 84:295-306.
- Brönmark, C., and Hansson, L. 2000. Chemical communication in aquatic systems: an introduction. *OIKOS* 88:103-109.
- Burks, R. L., Jeppesen, E., and Lodge, D. M. 2001a. Littoral zone structures as *Daphnia* refugia against fish predators. *Limnology and Oceanography* 46(2): 230-237.
- Burks, R. L., Jeppesen, E., and Lodge, D. M. 2001b. Pelagic prey and benthic predators: impact of odonate predation on *Daphnia*. *North American Benthological Society* 20(4): 615-628.
- Burks, R. L. and Lodge, D. M. 2002. Cued in: advances and opportunities in freshwater chemical ecology. *Journal of Chemical Ecology* 28:1901-1917.
- Carpenter, S.R., and Lodge, D.M. 1986. Effects of submersed macrophytes on ecosystem processes. *Aquatic Botany* 341-370.
- Cattaneo, A., Galanti, G., Gentinetta, S., and Romo, S. 1998. Epiphytic algae and macroinvertebrates on submerged and floating-leaved macrophytes in an Italian lake. *Freshwater Biology* 39: 725-740.
- Cronin, G. 1998. Influence of macrophyte structure, nutritive value, and chemistry on the feeding choices of a generalist crayfish. *The Structuring Role of Submerged Macrophytes in Lakes* 21: 307-317.
- Chick, J. H., and McIvor, C. C. 1993. Patterns in the abundance and composition of fishes among beds of different macrophytes: viewing a littoral zone as a landscape. *Canadian Journal of Fishery and Aquatic Science* 51:2873-2882.
- De Bernardi, R., and Peters, R. H. 1987. Why *Daphnia*? *Memorie dell' Instituto Italiano di Idrobiologia* 45:1-9.
- Diehl, S., and Kornijow, R. 1998. Influence of submerged macrophytes on trophic interactions among fish and macroinvertebrates. *The Structuring Role of Submerged Macrophytes in Lakes* 2: 24 – 46.
- Dorn, N. J., Cronin, G., and Lodge, D. M. 2001. Feeding preferences and performance of an aquatic lepidopteran on macrophytes: plant hosts as food and habitat. *Oecologia* 128(3): 406-415.
- Frodge, J. D., Thomas, G. L., and Pauley, G. B. 1990. Effects of canopy formation by floating and submergent aquatic macrophytes on the water quality of two shallow Pacific Northwest lakes. *Aquatic Botany* 38: 231-248.
- Jeppesen, E., Lauridsen, T. L., Kairesalo, T., and Perrow, M. R. 1997. Impact of submerged macrophytes on fish-zooplankton interactions in lakes. *The Structuring role of submerges Macrophytes in Lakes* 5:145-158.
- Kvam, O. V., and Kleiven, O. T. 1995. Diel horizontal migration and swarm formation in *Daphnia* in response to *Chaoborus*. *Hydrobiologia* 307: 177-184.

- Lauridsen, T. L., and Lodge, D. M. 1996. Avoidance by *Daphnia magna* of fish and macrophytes: Chemical cues and predator-mediated use of macrophyte habitat. *Limnology Oceanography* 41(4): 794-798.
- Lauridsen, T. L., Pedersen, L. J., Jeppesen, E., and Sondergaard, M. 1996. The importance of macrophyte bed size for cladoceran composition and horizontal migration in a shallow lake. *Journal of Plankton Research* Vol. 18(12): 2283-2294.
- Marklund, O., Blindow, I., and Hargeby, A. 2001. Distribution and diel migration of macroinvertebrates within dense suberged vegetation. *Freshwater Biology* 46: 913-924.
- Moss, B. 1998. Shallow lakes, biomanipulation and eutrophication. *Scope Newsletter* 29:2-27.
- Moss, B., Kornijow, R., and Measey, G. J. 1998. The effects of nymphaeid (*Nuphar lutea*) density and predation by perch (*Perca Fluviatilis*) on the zooplankton communities in a shallow lake. *Freshwater Biology* 39: 689-697.
- Ostrofsky, M. L., and Zettler, E. R. 1986. Chemical defenses in aquatic plants. *Journal of Ecology* 74: 279-287.
- Olson, E. J., Engstrom, E. S., Doeringsfeld, M. R., and Bellig, R. 1995. Abundance and distribution of macroinvertebrates in relation to macrophyte communities in a prairie marsh, Swan Lake, Minnesota. *Journal of Freshwater Ecology*, 10(4): 325-335.
- Schriver, P., Bøgestrand, J., Jeppesen, E., and Søndergaard, M. 1995. Impact of submerged macrophytes on fish-zooplankton-phytoplankton interactions: large-scale enclosure experiments in a shallow eutrophic lake. *Freshwater Biology* 33:255-270.
- Stich, H. B., and Lampert, W. 1984. Growth and reproduction of migrating and non-migrating *Daphnia* species under simulated food and temperature conditions of diurnal vertical migration. *Oecologia* 61: 192-196.
- White, M. D., 1998. Horizontal distribution of pelagic zooplankton in relation to predation gradients. *Ecography* 21: 44-62.
- Winfield, I. J., 1986. The influence of simulated aquatic macrophytes on the zooplankton consumption rate of juvenile roach, *Rutilus rutilus*, rudd, *Scardinius erythrophthalmus*, and perch, *Perca fluviatilis*. *Journal of Fish Biology* 29 (supplement A): 37-48.

Activation of GABA-B Receptors Attenuates N-type and Facilitates L-type Calcium

Currents in Isolated Hippocampal Neurons through Different Intracellular Mechanisms

A. Paydar, Rhodes College, Memphis, TN and M. Mynlieff, Marquette University, Milwaukee, WI

Introduction:

The GABA-B receptor pathway, which is activated by GABA neurotransmitter under normal physiological conditions, regulates synaptic neurotransmitter release by modulating calcium currents ($I_{Ca^{2+}}$) in both excitatory and inhibitory hippocampal neurons. Upon activation, this metabotropic pathway controls presynaptic calcium influx through high voltage activated (HVA) calcium channels (chiefly N- and L-type). Studies with specific channel antagonists have previously demonstrated that the GABA-B receptor activation produces two opposing effects on calcium conductance in these cells. It can distinctively attenuate $I_{Ca^{2+}}$ through N-type channels and facilitate, or increase, $I_{Ca^{2+}}$ through L-type channels. GABA-B induced attenuation of calcium influx through N-type channels, which mostly reside at the nerve terminal, plays a role in presynaptic autoinhibition of neurotransmitter release. On the other hand, GABA-B facilitation of calcium currents through L-type channels, which occupy the neuronal soma and proximal dendrites, governs such processes as enzymatic activity and gene expression. These discrete effects are often present simultaneously in a single cell (Carter and Mynlieff, 2001).

Many intracellular mechanisms for both N-type inhibition and L-type facilitation of $I_{Ca^{2+}}$ have been observed and proposed in different neuronal systems, all of which involve transmembrane G-protein activation (Table 1). Different subtypes of G-proteins are speculated to mediate this mechanism either by direct allosteric coupling with the calcium channels or, alternatively, by amplification or depression of second messenger molecules (e.g. cAMP and DAG), possibly resulting in an increase in activity of kinases, such as Protein Kinases A (PKA) or Protein Kinase C (PKC). The discrepancy between the previous findings is most likely due to

observations in different cell types. None of these experiments have specifically focused on the intracellular mechanisms for GABA-B regulation of HVA calcium channels in rat hippocampal neurons, particularly the inhibitory interneurons.

The present study investigates the specific intracellular pathways through which GABA-B receptor activation inhibits and facilitates N- and L-type calcium channels, respectively, in cultured hippocampal neurons. The effects of baclofen, a GABA-B agonist, on calcium currents in cultured rat pup hippocampal cells is examined in control cells and in cells treated with pertussis toxin, which permanently inactivates the G_i and G_o protein α -subunits, or RP-cAMP, which inactivates PKA.

Methods:

The heterogeneous excitatory and inhibitory neurons that constitute the superior region (CA1) of the hippocampus were initially isolated for electrophysiological recordings. As explained by Mynlieff, transverse hippocampal slices were obtained from 5-8 day old Sprague-Dawley rats (*Rattus norvegicus*) and later cultured (1997). After a 24-hour incubation period, whole cell patch clamp recording (voltage clamp mode) was carried out at room temperature on the isolated neurons with a DAGAN 3900A amplifier (DAGAN Corp, Minneapolis, MN), Digidata 1200 data acquisition system and PClamp 8.0 software (Axon Instruments, Forest City, CA; Carter and Mynlieff, 2001). Recording electrodes were made from borosilicate glass and had resistances of 4-8 M Ω when filled with 10mM CaCl₂, 145mM TEA-Cl, 10mM HEPES, 1 μ M TTX, pH 7.4. Cells were bathed in a 10 mM calcium based external solution (140mM CsAsp, 5mM MgCl₂, 10mM CsEGTA, 10mM HEPES, 2mM ATP-Na₂, 0.1mM GTP, pH 7.4). Calcium currents were elicited by a single 300ms depolarizing pulse to 10mV from a holding potential of -80mV or by successive 300ms depolarizing pulses from -50 to +50 mV in 10mV increments from a holding potential of -80mV.

The experiments in this study were conducted under three separate conditions. First, a control study was performed to examine the cultured cells' natural calcium current responses to GABA-B receptor activation. By using a U-tube system, 10 μ M baclofen was directly superfused onto the entire cell in the recording dish in order to specifically activate GABA-B receptors expressed by these cell (Carter and Mynlieff, 2001). Then, cultured dishes were incubated overnight (minimum of 16 hours) with the $G_{o\alpha}/G_i\alpha$ protein inactivator, pertussis toxin (PTX), prior to recording. 200ng/ml PTX was applied one hour after the cells were dissociated in culture. Finally, 50 μ M Rp-Adenosine 3',5'-cyclic onophosphorothioate triethylammonium (RP-cAMP) was infused into another population of cells by intracellular dialysis in order to inhibit PKA activity at the time of recording.

N-Type inhibition:

$GABA_B \rightarrow G_{o\alpha} \xrightarrow{\text{Direct Coupling}} \downarrow I_{Ca}$
(Clapham, 1994; Shen & Slaughter, 1999; Misgeld et al, 1995; Sweeney & Dolphin, 1992; Zhang et al, 1997; etc.)

$GABA_B \rightarrow G_{\beta\gamma} \xrightarrow{\text{Direct Coupling}} \downarrow I_{Ca}$
(Hille, 2001; Clapham, 1994; Zhou et al, 2000; etc.)

$GABA_B \rightarrow G_i\alpha \rightarrow \downarrow AC \rightarrow \downarrow cAMP \rightarrow \downarrow PKA \rightarrow \downarrow I_{Ca}$
(Hille, 2001; Bowery et al, 2002; Freissmuth, 1989; Misgeld et al, 1995; etc.)

$GABA_B \rightarrow G_s\alpha \rightarrow AC \rightarrow cAMP \rightarrow PKA \rightarrow \downarrow I_{Ca}$
(Carter & Mynlieff, 2001)

L-type facilitation:

$GABA_B \rightarrow G_{o\alpha} \xrightarrow{\text{Direct Coupling}} \uparrow I_{Ca}$
(Sweeney & Dolphin, 1992)

$GABA_B \rightarrow G_s\alpha \rightarrow AC \rightarrow cAMP \rightarrow PKA \rightarrow \uparrow I_{Ca}$
(Hille, 2001; Capogna et al, 1995; Obrietan & van del Pol, 1997; Kavalali et al, 1997; Clapham & Neer, 1993; etc.)

$GABA_B \rightarrow G_{\beta\gamma} / G_q\alpha \rightarrow PLC\beta \rightarrow DAG \rightarrow PKC \rightarrow \uparrow I_{Ca}$
(Hille, 2001; Clapham & Neer, 1993, Bartschat & Rhodes, 1995; Bowery et al, 2002; Shen & Slaughter, 1999).

Table 1: Possible intracellular pathways proposed by former experimentalists that may mediate N-type inhibition and L-type facilitation of I_{Ca2+} by GABA-B activation.

Results and Discussion:

The original inward currents traces evoked due to calcium influx at different time intervals during recording from a single cell (Figure 1A) are converted to voltage-current (IV) relationship curves that illustrate peak, sustained, and transient $I_{Ca^{2+}}$ as a function of an increasing membrane voltage (Figure 1B). These IV plots are used to determine the peak currents that show a prominent change in calcium currents due to the application of baclofen for all the patch clamped cells. Representative examples of cells that exhibit different responses (N-type inhibition, L-type facilitation, or no response) to baclofen are shown in peak current versus recording time graphs for the control, PTX, and RP-cAMP experiments (Figures 5-7 respectively). Linear regression lines in these graphs (fit with control and washout data points) exhibit the magnitude of change in currents during the application of baclofen for all the recorded cells. Consequently, the average percent changes in peak currents upon baclofen application for all three experimental conditions are determined (Figure 6).

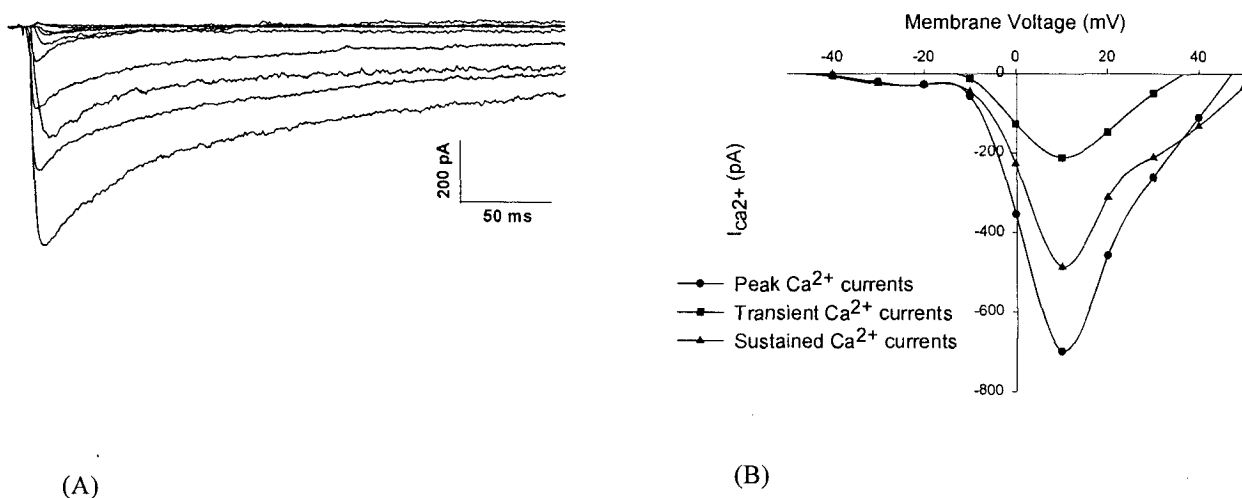


Figure 1: A) Inward calcium currents were elicited by a series of 300ms depolarizing pulses from -50mV to +50mV in 10mV increments from a holding potential of -80mV. B) A voltage versus current plot represents the peak current of recorded calcium traces, the sustained current (baseline current observed at the end of the traces), and the transient current (the difference between the peak and sustained currents in pA).

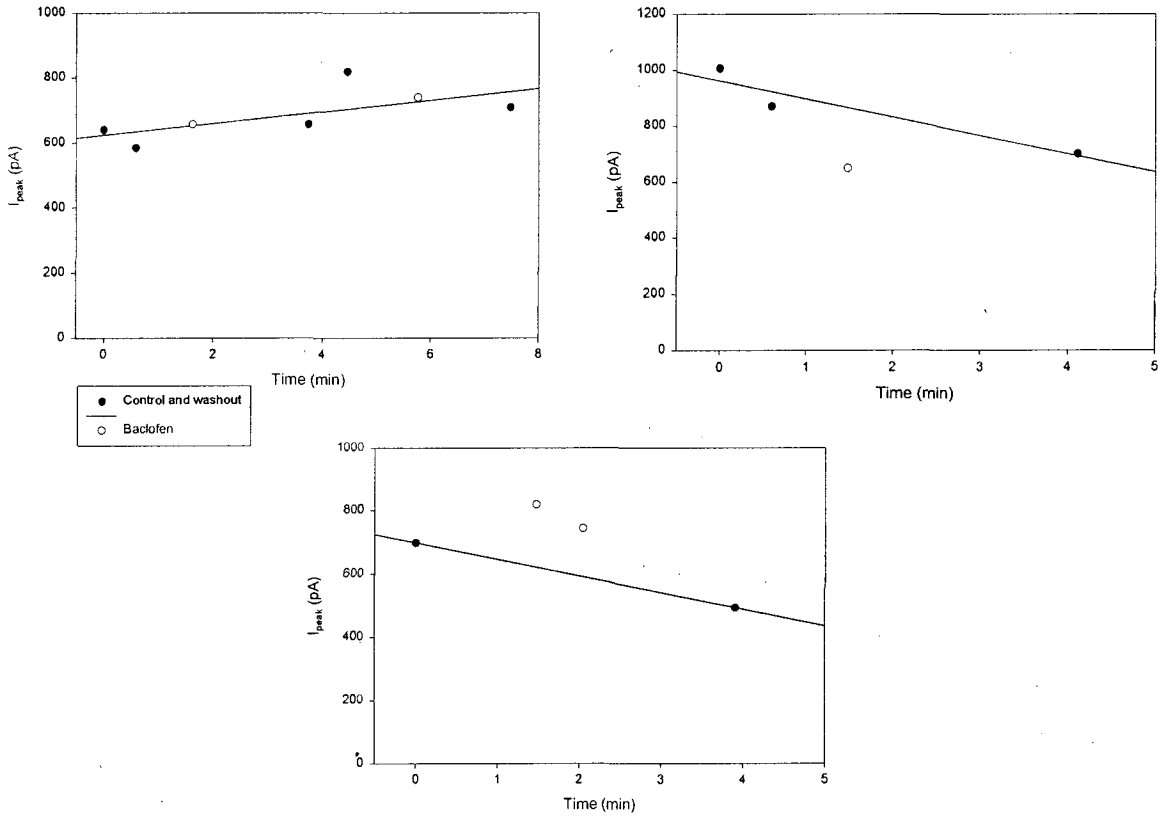


Figure 2: Time vs. current graphs show an example of a control cell exhibiting no response to baclofen, one showing inhibition, and one displaying facilitation of $I_{Ca^{2+}}$ (black points represent control and washout recordings and the white point represents recordings during baclofen application). Linear regression lines are produced using control and washout data points.

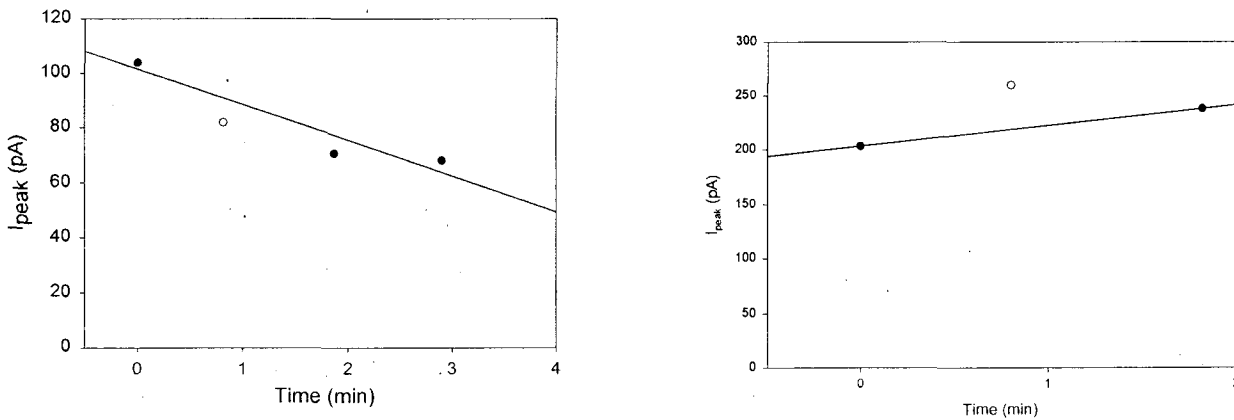


Figure 3: Time vs. current graphs show an example of a PTX-treated cell exhibiting no response to baclofen and one showing facilitation of $I_{Ca^{2+}}$ (black points represent control and washout recordings and the white point represents recordings during baclofen application). Linear regression lines are produced using control and washout data points.

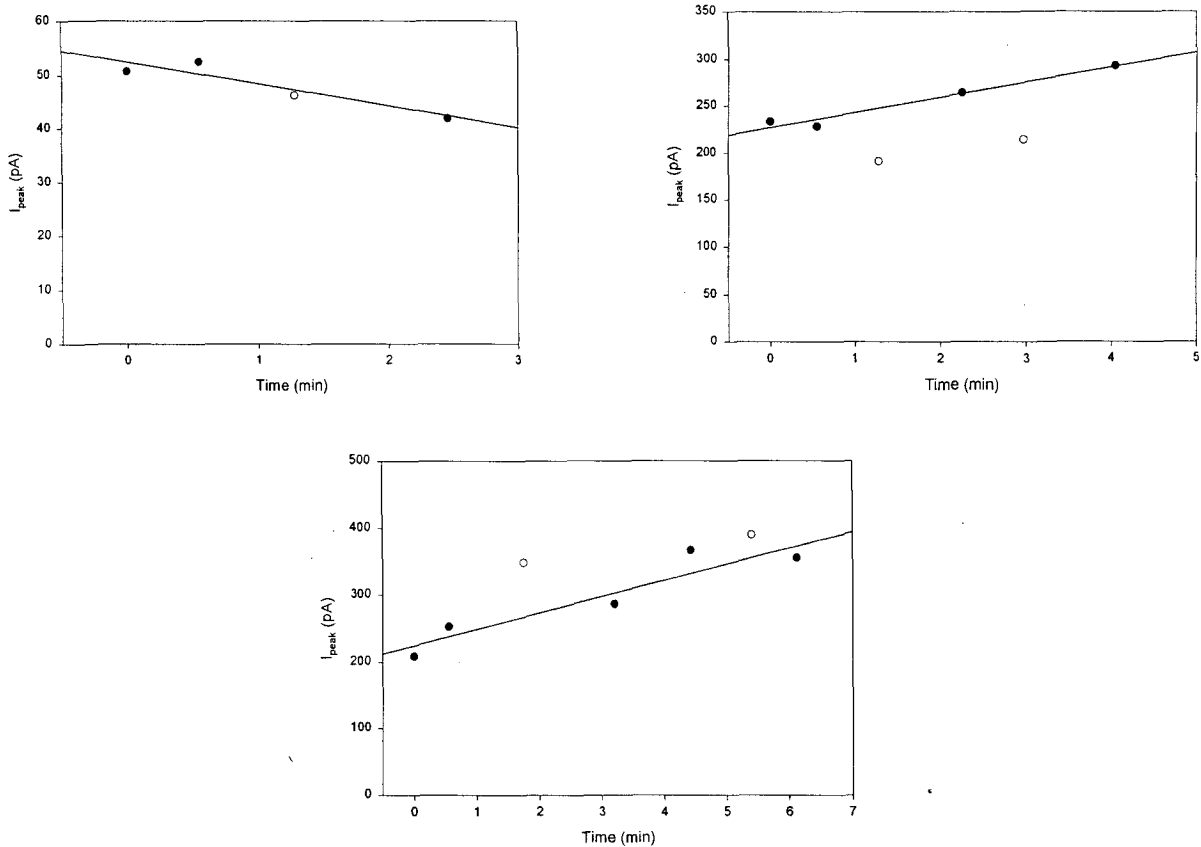
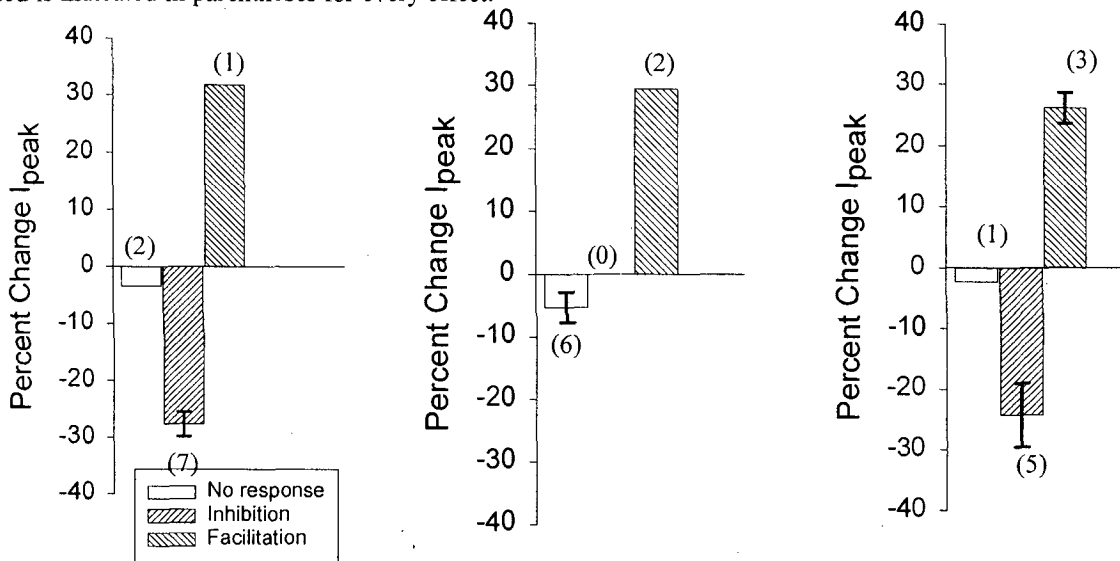


Figure 4: Time vs. current graphs show an example of a RP-cAMP-treated cell showing no response to baclofen, one exhibiting inhibition, and one displaying facilitation of $I_{Ca^{2+}}$ (black points represent control and washout recordings and the white point represents recordings during baclofen application). Linear regression lines are produced using control and washout data points.

Figure 5 Average percent changes in peak currents upon application of baclofen under control, PTX-treated, and RP-cAMP treated conditions are illustrated in the left, middle, and right graph respectively. The number of cells tested is indicated in parentheses for every effect.



The control experiment carried out in this study demonstrates the unmanipulated response of cells to the baclofen-induced GABA-B activation. Control results contain 2 cells showing no statistically significant response to the application of baclofen (-3.33%), 6 cells exhibiting inhibition ($-7.60\% \pm 2.16$), and 1 cell displaying facilitation of calcium currents (31.73%; Figure 5). Former investigations of GABA-B modulation of I_{Ca2+} in heterogeneous hippocampal cell populations show similar results. Carter and Mynlieff have identified that 15% of cells non-responsive to baclofen, 54% demonstrating inhibition, and 30% exhibiting facilitation of peak I_{Ca2+} (2001). These different responses to GABA-B activation may reflect the complement of Ca^{2+} channels in different cell types or differential coupling between the GABA-B receptors and various second messenger systems. In other words, this data account for the heterogeneity of the various cell types in the hippocampal cultures that use various types of Ca^{2+} channels and signal transduction systems, and thus, response differently to baclofen.

Results from the PTX experiment provide evidence as to whether $G_i\alpha$ or $G_o\alpha$ protein subtypes are involved in the GABA-B metabotropic pathway that leads to N-type inhibition or L-type facilitation of I_{Ca2+} . In this study, six cells exhibit no statistically significant response to baclofen ($-5.25\% \pm 2.42$), 0 cells demonstrate inhibition, and 2 cells display facilitation (29.33%; Figure 5). These data suggest that N-type inhibition of I_{Ca2+} is hindered by PTX's inactivating $G_o\alpha/G_i\alpha$ protein subunits, verifying that N-type inhibition is probably mediated by $G_i\alpha$ or $G_o\alpha$ rather than by $G_s\alpha$, $G_q\alpha$, or $G\beta\gamma$ subunits. L-type facilitation of I_{Ca2+} , however, is not affected by PTX application, suggesting that the signal transduction pathway that results in facilitation does not depend on a PTX-sensitive G_i/G_o -protein subtype. These results are supported by findings of Clapham (1994), Shen & Slaughter (1999), Hill (2001) and many others. Accordingly, attenuation, and not facilitation, of I_{Ca2+} by GABA-B receptors is mediated by a PTX sensitive G-protein (G_i or G_o).

The experiment with Rp-cAMP investigates the involvement of PKA activity in the GABA-B modulatory pathway, allowing us to eliminate more possibilities of the proposed mechanisms of GABA-B inhibition and facilitation. In the PKA inhibition study, 2 cells demonstrate no statistically significant response to baclofen (-2.26%), 4 cells exhibit inhibition (-24.21% \pm 5.28), and 3 cells demonstrate facilitation (26.08% \pm 2.51; Figure 6). Evidently, neither inhibition nor facilitation is affected by RP-cAMP's PKA blocking capacity since these results are very similar to the control data. Thus, according to these results, it is likely that kinase activity by PKA, in particular, does not play a major role in intracellular modulation of I_{Ca2+} by GABA-B receptors in hippocampal neurons, regardless whether it is a decrease or an increase in kinase activity. These findings are specifically in accordance with and supported by the observations of many others (Clapham and Neer, 1993; Bartschat and Rhodes, 1995). Nonetheless, it has been formerly proposed that PKA activity may still play a minor role in facilitation of L-type channels (Shen and Slaughter, 1999).

In conclusion, after refuting certain formerly proposed mechanisms and supporting others, our findings suggest that inhibition of I_{Ca2+} by activation of GABA-B receptors is most likely through direct allosteric coupling of G_o proteins with N-type calcium channels (Table 2). In addition, GABA-B I_{Ca2+} facilitation may be primarily linked to PKC kinase activity that leads to activation of L-type channels through internal phosphorylation; although PKA might still play a minor role in this pathway (Table 2). More studies need to be performed to confirm these results. More cell recordings need to be carried out for each of these experiments to reduce the sampling error. The PKA inactivation data (RP-cAMP experiment) may also be confirmed by using another type of PKA inhibitor. Furthermore, other pharmacological manipulations need to be directed towards other G-proteins, second messenger molecules, and protein kinases to

eliminate other possibilities of how the GABA-B receptor modulates these HVA $I_{Ca^{2+}}$ in hippocampal neurons.

N-Type inhibition:

$GABA_B \rightarrow G_{\alpha} \xrightarrow{\text{Direct Coupling}} \downarrow I_{Ca}$
(Clapham, 1994; Shen & Slaughter, 1999; Misgeld et al, 1995; Sweeney & Dolphin, 1992; Zhang et al, 1997; etc.)

L-type facilitation:

$GABA_B \rightarrow G_{\beta\gamma} / G_{q\alpha} \rightarrow PLC\beta \rightarrow DAG \rightarrow PKC \rightarrow \uparrow I_{Ca}$
(Hille, 2001; Clapham & Neer, 1993, Bartschat & Rhodes, 1995; Bowery et al, 2002; Shen & Slaughter, 1999)

Table 2: Experimentally supported GABA-B receptor metabotropic pathways that distinctively modulate N- and L-type HVA calcium channels in the hippocampal neuronal system.

References:

- Bartschat, D. K. & Rhodes, T. E. (1995). Protein kinase C modulates calcium channels in isolated presynaptic nerve terminals of rat hippocampus. *J. of Neurochem.* 64, 2064-2072.
- Capogna, M., Gähwiler, B. H., & Thompson, S. M. (1995). Presynaptic enhancement of inhibitory synaptic transmission by protein kinase A and C in the rat hippocampus *in vitro*. *J. of Neurosci.* 15(2): 1249-1260.
- Carter, T. J. & Mynlieff, M. (2001). GABA-B receptors attenuate and facilitate calcium currents in hippocampal neurons. Society for Neuroscience, Vol. 27.
- Clapham, D. E. (1994). Direct G-protein activation of ion channels? *Annu. Rev. Neurosci.* 17:441-64
- Clapham, D. E. & Neer, E. J. (1993). New roles for G-protein beta-gamma-dimers in Transmembrane signaling. *Nature* vol. 365.
- Freissmuth, M., Casey, P. J., & Gilman, A. G. (1989). G-proteins control diverse pathways of transmembrane signaling. *FASEB J.* 3:2125-2131.
- Hartzell, H. C. & Fischmeister, R. (1992). Direct regulation of cardiac calcium channels by G-proteins: neither proven nor necessary? *Trends Pharmacol. Sci.* 13(10): 380-85.
- Hille, Bertil (2001). *Ion Channels of Excitable Membranes: Third Edition*. Sunderland, MA: Sinauer Associates.
- Kavalali, E. T., Hwang, K. S., & Plummer, M. R. (1997). CAMP-dependent enhancement of dihydropyridine-sensitive calcium channel availability in hippocampal neurons. *J. of Neurosci.* 17(14): 5334-5348.
- Misgeld, U., Bijak, M., & Jarolimek, W. (1995). A physiological role for GABA-B receptors and the effects of baclofen in the mammalian central nervous system. *Prog. in Neurobio.* Vol. 46, pp. 423-462.
- Mynlieff M. Dissociation of postnatal hippocampal neurons for short term culture. *J. Neurosci Methods* 73:35-44, 1997.
- Obrietan, K. & van den Pol, A. (1997). GABA activity mediating cytosolic calcium rises in developing neurons is modulated by cAMP-dependent signal transduction. *J. of Neurosci.* 17(12): 4785-4799.
- Shen, W. & Slaughter, M. M. (1999). Metabotropic GABA receptors facilitate L-type and inhibit N-type calcium channels in single salamander retinal neurons. *J. of Phys.* 516.3, pp. 711-718.
- Sweeney, M. I., & Dolphin, A. C. (1992). 1,4-Dihydropyridines modulate GTP hydrolysis by G_{α} in neuronal membranes. *FEBS* vol. 310, no. 1, pp. 66-70.
- Zhang, J., Shen, W., & Slaughter, M. (1997). Two metabotropic gamma-aminobutyric acid receptors differentially modulate calcium currents in retinal ganglion cells. *J. Gen. Physiol.* vol. 110, pp. 45-58.
- Zhou, J. Y., Siderovski, D. P., & Miller, R. J. (2000). Selective regulation of N-type calcium channels by different combinations of G-protein beta/gamma subunits and RGS proteins. *J. of Neurosci.* 20(19):7143-7148.

Supported by NIH 01R29NS33012 and NSF 0139061

Quantitative Real-Time RT-PCR Assay

Shauna Torrence

ABSTRACT

Background: To evaluate potential anti viral treatment strategies and to understand RSV pathogenesis requires quantitative tests for RSV. Currently, this is determined by quantitative culture (plaque assay); however, real-time quantitative RT-PCR theoretically offers the potential advantages of increased sensitivity, stability of the assay after specimen freeze/thaw, and low cost. These potential advantages would facilitate multi-center studies of pathogenesis and therapeutic trials.

Methods: The GenBank Database, was searched to locate conserved regions within the RSV genome. Due to relatively low homology between strains A and B, these strains were separated and homologous regions within each strain were analyzed to find appropriate primers and probes. A quantitative viral RNA extraction protocol was developed for use on nasal washings followed by reverse transcription and subsequent real-time PCR reaction using ABI 7900HT. Primers and probes from regions of the N gene and F gene were developed. RSV A patient aliquots which had been frozen for >1 year at -80°C , but had been quantified fresh using plaque assay were analyzed. Values were extrapolated from standard curves prepared by parallel RNA extraction of RSV-A long quantitative standards.

Results: The predicted quantity of RSV as measured by real-time RT-PCR using RSV-A N gene in spiked nasal washings correlated well with predicted values ($R^2=0.9560$) ($n=8$). The lower limit of detection was $10^{1.15}$ PFU/mL. The quantity of RSV from supernatants of HEp-2 cells infected with individual patient isolates measured by real-time RT-PCR correlated with that measured by fresh plaque assay ($R^2=0.866$) ($n=22$). The quantity of RSV in direct patient specimen (respiratory secretions) was measured by real-time RT-PCR. Intra assay precision was high ($R^2=0.961$, $n=35$). Results correlated with that measured by fresh plaque assay ($R^2=0.296$) ($n=35$) ($P=0.0007$). Mean values in log PFU equivalents/mL were 1.31 times higher than those obtained by plaque assay.

Conclusions: Real-time RT-PCR appears to provide sensitive and reliable quantitative assessment of RSV A strains in frozen patient specimens, correlating with existing fresh plaque assay values. Further evaluation

is necessary to define the kinetics of RSV using this assay and to compare the plaque assay with the real-time RT-PCR assay under the influences of neutralizing antibodies and other antiviral experimental therapeutics.

INTRODUCTION

Respiratory syncytial virus (RSV) is the most common cause of lower respiratory tract infections in infants. In the United States, RSV hospitalizes 3% of all previously healthy infants within their first year of life [1], and the rate is increasing [2]. RSV has now become the single most common cause of hospitalizations in infants less than two years of age [3]. The virus, characterized by bronchiolitis, which causes wheezing, lung hyperexpansion and hypoxia, and is often associated with pneumonia, occurs in annual outbreaks in the winter months of temperate climates.

RSV is known to be a single-strand RNA virus that targets the respiratory epithelium, but the general pathogenesis is not well understood. It is thought that disease is due to both direct cytopathic effects of the virus and a pathogenic proinflammatory response [4,5]. There is no vaccine for RSV, and the only FDA-approved drug treatment currently available, aerosolized ribavirin, provides only moderate reduction of RSV concentrations, with the clinical benefits remain debatable [6]. Although clinical research has shown a direct correlation between the quantity of RSV present in the patient and disease severity, the theoretic utility of any antiviral treatment remains in doubt [6]. However, determining the success of this type of treatment requires the accurate ability to measure viral load in respiratory secretions.

Quantitative culture is the current method used in determining viral load of clinical samples. Reverse transcription polymerase chain reaction (RT-PCR) may offer several potential advantages in determining viral load including an increase in sensitivity and dynamic range, stability after freeze/thawing patient specimen thus facilitating multi-center trials, low cost, and the inability of neutralizing antibodies and experimental antivirals used in RSV therapy to affect this assay.

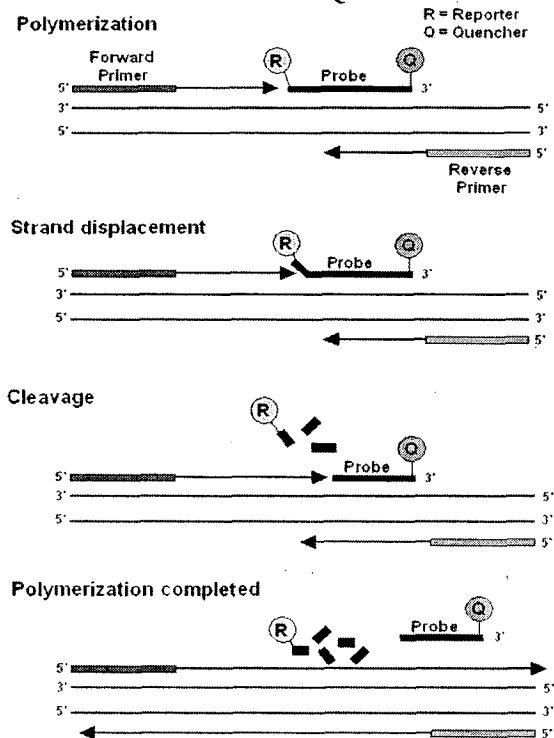
PCR does however present some problems in the quantification of RSV in that the final concentration of amplicon does not reflect the starting concentration of DNA. This disadvantage has been overcome with the development of real-time PCR, a technique that can perform amplification, detection and quantification all in one closed system as the amplification cycles are ongoing [7,8]. The 5' and 3' ends of the probe are linked

respectively to a 6-FAM reporter (6-carboxyfluorescein) and a TAMRA quencher (6-carboxytetramethylrhodamine) (**Figure 1**). As the Taq polymerase begins transcription, its 5' endonuclease activity begins to digest the probe, releasing the reporter from its proximity to the quencher such that the fluorescence can be detected. This increases as the PCR products accumulate. At a certain point during amplification, there is an exponential accumulation of PCR product (fluorescence) detected at differing time intervals within each reaction tube. This is known as the threshold cycle (C_t), the point at which the amount of fluorescence rises exponentially above the background. There is a linear relationship between the C_t and the log of the starting amount of DNA template.

Due to the need for viral quantification in the study of RSV pathogenesis and control as well as the potential advantages of real-time RT-PCR for quantification of RSV, we sought to design, develop, and validate such an assay.

MATERIALS AND METHODS

Figure 1: Process of Absolute Quantification



Quantitative Culture by Plaque Assay

Hep-2 cells at 80% confluency were placed in 12 well plates. The plates were then inoculated with ten-fold serial dilutions in triplicate. After one hour incubation at 37°C, methylcellulose media was added to the plates. The plates were allowed to incubate for five days and were then fixed and stained with Eosin. The plaques were counted using an inverted light microscope.

Creation of RSV Standards

A passage of HEP-2 cells was inoculated with an aliquot of lab strain RSVA-long. After five day incubation, allowing for optimal cytopathic effect on the cells, the supernatant was removed, aliquoted, and frozen at -70°C to preserve the RSV. A fresh plaque assay was run on one aliquot of the supernatant to determine the viral concentration of the RSVA-long strain prior to freeze/thawing at differing serial dilutions. A second assay

was run on a frozen aliquot of the same viral strain to determine parallel quantitative culture between fresh and frozen samples. The concentration generally achieved is approximately 10^7 plaque forming units per milliliter (PFU/ml) and is the value assigned to our lab standard. Parallel aliquots were also used for real-time RT-PCR to allow for comparison of fresh plaque assay and the effects of freeze-thawing on real-time RT-PCR results.

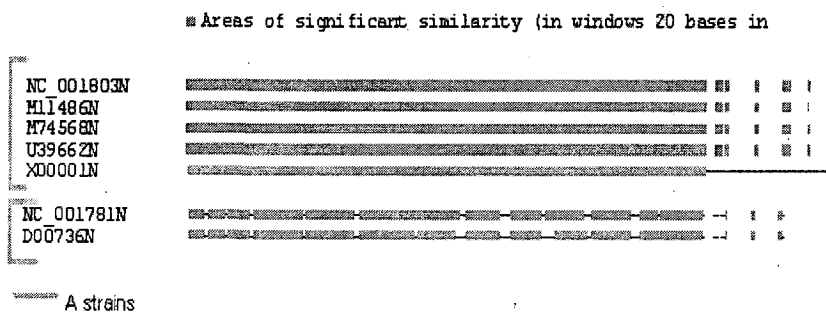
Human Subjects and Clinical Specimens

Respiratory secretions were collected by members of the research team in a standardized manner and placed immediately in a RSV stabilization media on wet ice. Quantitative cultures were initiated with fresh respiratory secretions within four hours of collection. Subjects were identified using RSV DFA or Directigen® (Becton

Dickinson, Franklin Lakes, NJ), an available, rapid RSV diagnostic test.

Subjects were enrolled if they were RSV positive and were < 2 years of age. They were excluded if they had congenital heart disease, immunodeficiency, and chronic lung

Figure 2: Significant Similarity Map of N Gene A and B Strains



disease or had received corticosteroids (conditions thought to disturb the relationship between RSV load and disease severity. The Institutional Review Board of the University of Tennessee approved all activities.

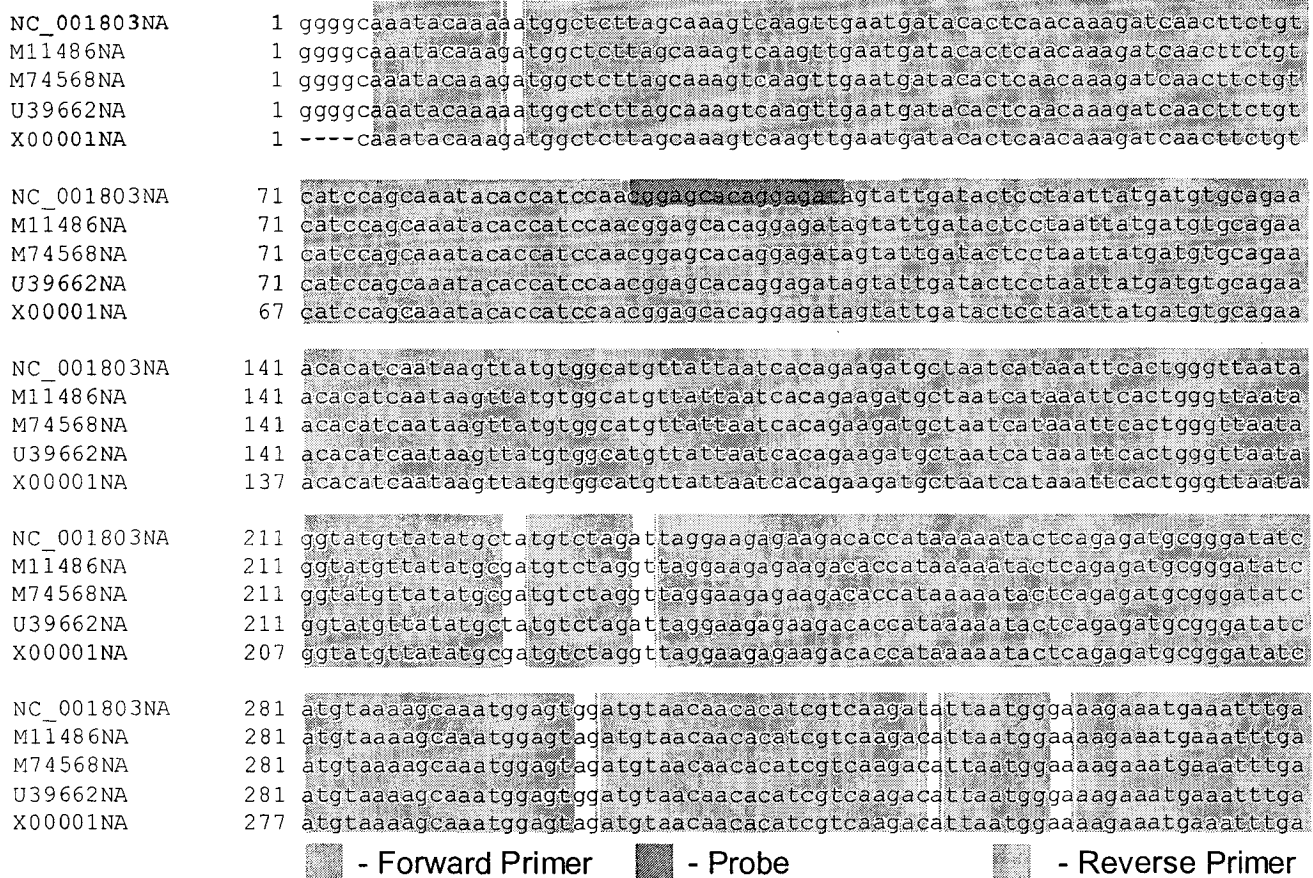
Selection of Primers and Probes

All available nucleotide sequences of both RSVA and RSVB wild type strain genomes were accessed from the GeneBank database. Experimentally mutated strains were excluded. All genes were then aligned and analyzed for areas of significant homology within each gene of the GeneBank strains using Clone Manager Suite™ (Figure 2). It is necessary to conserve complete homology between the differing strains of both RSVA and RSVB to ensure amplification kinetics are the same, which is necessary for accurate absolute quantification for all wild type strains. There were no regions in which strains from both the RSVA and RSVB subgroups were completely homologous therefore the subgroups were analyzed separately to determine the most appropriate sites for primers and probes. Although some of the genes within each subgroup were discarded due to insufficient

areas of homology with in each wild type strain, such genes as N, L, and F showed sufficient regions of homology and were studied further.

Homologous areas of N, L, and F gene were analyzed for areas of complete homology and for primer and probe placement using Primer Express® (Applied Biosystems). This was done for each of these genes within each strain of both subgroups (RSV-A and RSV-B). The program was set to look for TaqMan® minor groove

Figure 3: Conserved Region of N Gene (A Strains)



binding primers and probes. The procedure was successful for both the N and F genes. Primer pairs and probes were found with appropriate predicted annealing and melting temperatures for both the N and F genes (RSV N-gene shown only, **Figure 3**).

Viral RNA Extraction and Reverse Transcription

RSV vRNA was extracted using a QIAamp® Viral RNA Mini Kit (Qiagen, Valencia, CA) utilizing centrifugation and the unique binding properties of silica, which elutes at least 90% of the viral RNA from the sample.

Reverse Transcription was performed using Omniscript™ Reverse Transcriptase and the primer for RSV A N gene (5'-ATGGCTCTTAGCAAAGTC-3'). The RT sample was allowed to incubate at 37°C for one hour followed by reverse transcriptase inactivation at 95°C for 5 minutes. The samples were then immediately placed on ice.

Real-Time RT-PCR

Frozen aliquots of RSV-A long standards were run in a 96 well plate in five 10-fold serial dilutions using an ABI Prism® 7900HT Sequence Detection System (Applied Biosystems International). The primers and probes created for the RSV-A N gene are listed as follows: forward primer-5'-

CTGTCATCCAGCAAATACACCATCCA-3', reverse primer-5'-

TTCTGCACATCATAATTAGGAGTATCAA-3', and probe-5'CGGAGCACAGGAGAT-3' (**Figure 3**).

Following reverse transcriptase inactivation, reaction mixtures of 25µl were analyzed in triplicate, which consisted of: 900nM forward primer, 900nM reverse primer, 250nM probe, 12.5µl 2X TaqMan® Universal PCR Master Mix, 5.0µl template cDNA, and 0.5µl of RNase-free water. Each PCR reaction plate also contained a negative control in which water was substituted for cDNA. The reaction was carried out under the following thermal dynamic cycle parameters: 2 minutes at 50°C, 10 minutes at 95°C, 40 cycles of 15 second intervals at 95°C and one minute at 60°C.

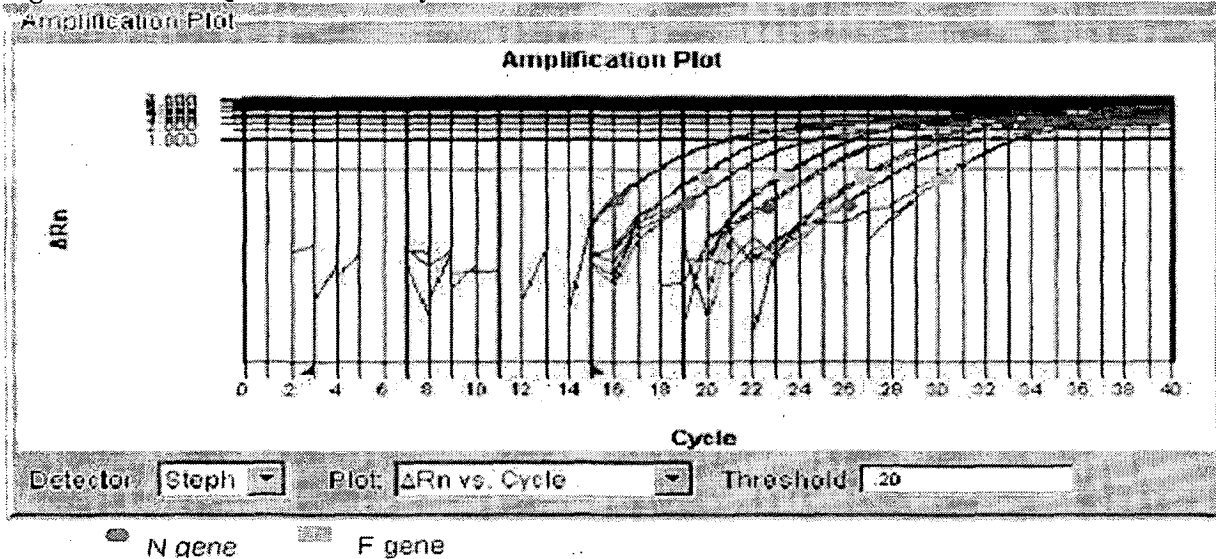
Standard curves were constructed based on the cycle threshold results of the real-time RT-PCR reaction as compared to the known PFU/ml obtained from quantitative culture of fresh plaque assay. The standard curves were used to interpolate the starting vRNA concentrations in log PFU equivalents/ml (PFUe/mL) of the unknown patient samples.

RESULTS

Quantification of RSVA-long Standards Using the F and N Genes

A set of four RSVA-long standards were quantified using real-time RT-PCR for both the N and F genes. The amplification plot of the C_t values for the N gene read 2.22-2.29 equivalents lower than those of the F gene. Quantitative culture by fresh plaque assay suggests that each equivalent of standard produces the same PFU/ml,

Figure 4: RSVA Quantification by N Gene and F Gene



where as the RT-PCR assay was more sensitive for the N gene, causing the two to have differing PFUe/ml. (Figure 4). Because of this increased sensitivity of N gene PCR, this gene target was used in the remaining experiments.

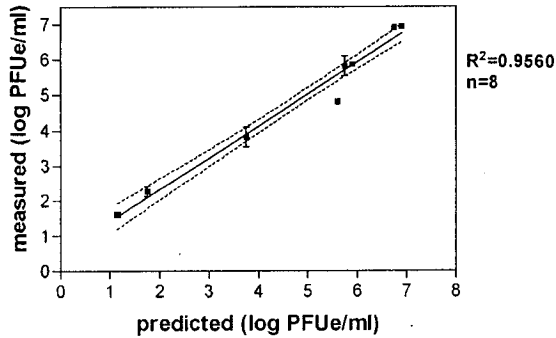
Testing for RNA Extraction Efficiency and RT-PCR Inhibitors

Nasal wash fluid not containing RSV was spiked with eight different quantities of RSV-A long and was subsequently analyzed by real-time RT-PCR. This allowed for verification that our RNA extraction procedure was able to successfully extract and detect RSV virus from thick patient nasal secretions. The results correlated highly with the predicted RSV concentration in the spiked Nasal Wash fluid ($R^2=0.9560$) (See Figure 5). Due to the tight correlation, RNA extraction efficiency appears high and PCR inhibition appears not to be occurring. A negative control was assayed using a sample of RSVB strain resulting in no detection of RSVB by RSVA primers and probes.

Quantification of Cultured Patient Isolates by N gene

Twenty-two wild type patient RSV A isolates were cultured in Hep-2 cell monolayers.

Figure 5: Correlation of RSV A PCR in Spiked Nasal Washes



Supernatants from these cultures were then quantified by fresh plaque assay. Other aliquots were frozen at -80°C and then tested by real-time RT-PCR. There were excellent correlation results between the results obtained by the plaque assay and that obtained by PCR ($R^2=0.866$) (See **Figure 6**). Thus a sizeable number of different wild type

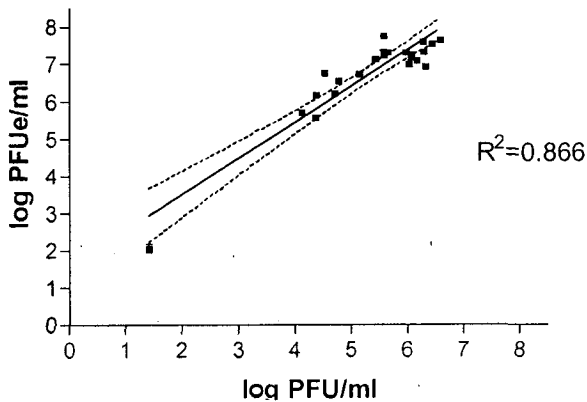
strains of RSV appear to be quantitatively detectable using this real-time RT-PCR assay.

Direct Quantification from Infants Respiratory Secretions

Thirty-five frozen patient samples, previously quantitatively cultured by fresh plaque assay, were analyzed using real-time RT-PCR. Real-Time RT-PCR correlated with plaque assay in these clinical

nasal washes ($R^2=0.296$) (See **Figure 7**). The dashed line represents 95% confidence intervals for the calculated slopes of the regression line ($P=0.0007$ for slopes not representing zero).

Figure 6: Correlation of Cultured Patient Isolates vs. Real-Time RT-PCR for the N gene



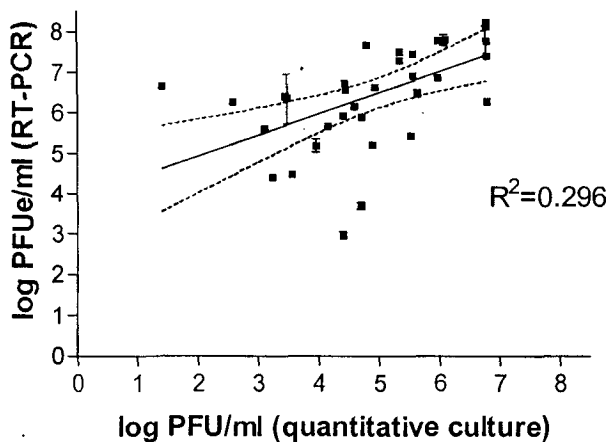
Determination of Real-Time RT-PCR Assay

Precision

In order to determine precision of the

PCR assay, each patient specimen was run in duplicate in the 96 well plates. There is excellent intra assay precision based on tight correlation between the two PCR wells for each of the thirty-five patient specimens ($R^2=0.961$) (See **Figure 8**).

Figure 7: Correlation of Patient Respiratory Secretions: Culture vs. Real-Time RT-PCR N gene



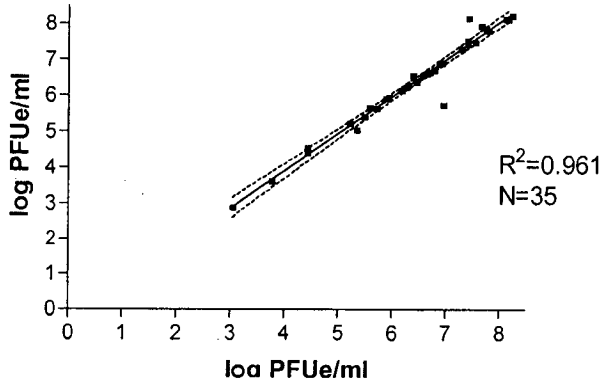
DISCUSSION

The real-time RT-PCR assay appears to have good correlating results for spiked nasal wash patient specimen with known quantities for RSVA-long standard. Therefore, we felt that the extraction of the vRNA is successful using our current protocol. It might be possible in the future to use random primers for the reverse transcription step; however, our results using our specific primers have given us no reason to change our procedure at this time.

For the PCR tests run on the supernatant of cultured patient isolates, the assay produced tight correlation with quantitative culture. Yet the PCR quantification of freeze/thawed direct patient specimens produced a much wider spread. It is possible that the supernatant of the cultured patient samples produced a tighter correlation because the sample is more pure, less viscous and does not contain any inhibitors that might be present in a patient's respiratory secretions. Although, our results on spiked nasal wash samples lead us to believe that inhibitors do not affect the assay, it is possible that inhibitors such as increased mucus produced in the infected patient might have some affect on the correlation between PFUe/ml and PFU/ml.

Another reason for the wider spread observed in direct patient specimens is that the quantitative PCR

**Figure 8: Precision of Assay in Patient Respiratory Secretions:
Correlation of PCR vs. PCR**



assay actually detects both infectious virus, viral particles and free RNA, whereas the plaque assay does not contain any means for accounting for the presence of viral particles. This includes infectious viruses, which are not able to form plaques, non-infectious viral particles, and any fragments, which might contain our desired N-gene target. The rate of RSV RNA clearance in clinical samples and the elimination half-life of

its RNA are not known. It is likely that the PCR yields a wider spread for the patient samples because of the variable ratios of infectious virus to viral particles in the patient specimens, and the ability of this assay to measure non-infectious particles. Although the tests run on the patient samples produced a wide spread, we felt confident in the precision of our assay due to the tight correlation between the duplicate wells of each patient sample in the quantitative PCR assay.

Real-time RT-PCR does overcome many of the disadvantages presented by plaque assay in that it is less labor intensive, is more cost efficient, and eliminates some of the problems associated with non-sterile collection sites. Nevertheless, there are limitations to our data. The assay does, however, possess difficulties of its own. The correlating results of the quantitative PCR assay are presented in PFU equivalents. Currently, the most commonly used quantitative technique employed RSV therapeutics is the plaque assay. Therefore, most clinical experience is with this assay. In order to incorporate this experience, we chose to measure the real-time RT=PCR results in plaque forming unit equivalents (PFUe/ml). An area of further research is to use standards of known viral particle concentrations. This can be done through the use of quantitative electron microscopy. Alternatively, quantifying the PCR with respect to the number of RNA copies per ml could be accomplished through the use of N gene cloned into plasmids and used as standards.

Another limitation of our studies was that we only tested for RSV-A subgroup viruses. It is possible to run multiplex assays of both RSVA and RSVB in the same reaction tubes using RSV-A specific primers and

probe in conjunction with RSVB specific primers and probe. However, detection must be at two different wavelengths in the presence of both RSVA and RSVB standards. We feel that this would be both labor intensive as well as expensive because the wells used for unknown patients samples would be sacrificed for the dilutions of the two separate standards. Fluorescent antibody staining is an efficient and accurate way of differentiating between the two subgroups prior to quantitative PCR assay, and we do not feel altering the current technique would improve our results at this time. Further research is necessary to establish a reliable PCR assay for RSVB.

Future research directions include establishing the kinetics of RSV concentrations by quantitative PCR assay in individual patients over time. At the time of hospital admission, which most often occurs late in the infant's disease, the RSV concentrations are actually declining. If the elimination kinetics of RSV RNA are slower than for infectious virus, quantitative PCR might reflect RSV concentrations for earlier times in the disease process, thus providing additional insight into RSV pathogenesis and the potential usefulness of early antiviral therapy. Research is also needed to compare the plaque assay with PCR assay in the presence of anti-virals and neutralizing antibodies. This might also provide insight into the utility of an antiviral. In conjunction with looking into the correlation clinical samples from both nasal washes and tracheal aspirates might provide insight into developing an effective anti viral. Based on this research and future research directions, real-time RT-PCR could prove to be instrumental in allowing doctors to predict disease severity through fast and accurate determination of viral load as well as for multi-center antiviral therapeutic trials involving this severe infant disease.

Acknowledgements:

The author wishes to thank Dr. John DeVincenzo for his wonderful guidance, Stephanie Mabry and Kathy Kenwright for informative technique instructions, and is grateful for the unlimited assistance of Lisa Harrison and Jody Aitken in collection of the data presented. The author also appreciates the parents and the infants who participated in this study.

WORKS CITED

1. Boyce TG, Mellen BG, Mitchel EF, Jr., Wright PF, Griffin MR. Rates of hospitalization for respiratory syncytial virus infection among children in medicaid. *Journal of Pediatrics*. 2000;137:865-70
2. Shay DK, C HR, D NR, Liu LL, Stout JW, Anderson LJ. Bronchiolitis associated hospitalizations among US children, 1980-1996. *JAMA* 1999;282:1440-1446
3. Leader S, Kohlhase K. Respiratory syncytial virus-coded pediatric hospitalizations, 1997 to 1999. *Pediatric Infectious Disease Journal*. 2002;21:629-32
4. Hoebee B, Rietveld E, Bont L, et al. Association of severe respiratory syncytial virus bronchiolitis with interleukin-4 and interleukin-4 receptor alpha polymorphisms. *Journal of Infectious Diseases*. 2003;187:2-11
5. Polack FP, Teng MN, Collins PL, et al. A role for immune complexes in enhanced respiratory syncytial virus disease. *Journal of Experimental Medicine*. 2002;196:859-65
6. DeVincenzo JP. Therapy of respiratory syncytial virus infection. *Pediatr Infect Dis J* 2000;19:786-90
7. Houg HH, Hirtz D, and Kanesa-thasan N. Quantitative detection of dengue 2 virus using fluorogenic RT-PCR based on 3'-noncoding sequence. *J Virol Methods* 2000;86(1):1-11
8. Bustin SA. Absolute Quantification of mRNA using real-time reverse transcription polymerase chain reaction assays. *J Mol Endocrinol* 2000;25:169-193